

4 Magnetic Resonance Imaging in Kidney Cancer

E. SCOTT PRETORIUS

CONTENTS

4.1	Introduction	51
4.2	General Technical Considerations	52
4.3	Goals of Oncologic Renal MR Imaging Examinations	52
4.3.1	Renal Lesion Detection	52
4.3.2	Renal Lesion Characterization	53
4.3.3	Staging of Renal Cell Carcinoma by MR Imaging	56
4.3.4	Therapy Planning	58
4.3.5	Post-Therapy Imaging	59
4.4	Suggested MR Imaging Protocol	61
4.4.1	Localizer Images	61
4.4.2	T1-Weighted Images	61
4.4.3	T2-Weighted Images	62
4.4.4	Pre- and Post-Contrast Imaging	63
4.4.5	Subtraction Imaging	64
4.4.6	Functional Renal MR Imaging	64
4.4.7	MR Angiography	64
4.4.8	MR Venography	66
4.4.9	Flow-Related Vascular MR Imaging	67
4.4.10	MR Urography	68
4.5	Conclusion	71
	References	71

4.1 Introduction

Magnetic resonance (MR) imaging protocols for evaluation of patients with known or suspected renal malignancies have evolved with advancements in pulse sequences, surface coils, gradient magnets, and scanners. With improving MR imaging technology and increased radiologist experience, former limitations of relatively long imaging times and associated motion artifacts have largely been overcome. This has allowed renal diagnostic imagers to take fuller advantage of the many intrinsic advantages of MR imaging.

The single greatest advantage of MR imaging over ultrasound (US) and computed tomography (CT) is that MR imaging generates the highest intrinsic soft tissue contrast of any cross-sectional imaging modality. Furthermore, whereas both US and CT have a single basis for generating tissue contrast, the ever-broadening array of MR imaging pulse sequences continues to expand our imaging armamentarium.

Like US, MR imaging is capable of directly imaging in any plane, although of course MR imaging does not suffer from the tissue-depth penetration limitations of US. The CT data acquisition remains limited to the axial plane, although reconstructed data from multidetector-row scanners can provide excellent resolution in interpolated planes. Although MR imaging's spatial resolution remains inferior to that of CT, in the vast majority of renal cases this limitation is more than compensated for by MR imaging's superior contrast and multiplanar capabilities.

Renal MR imaging is particularly useful for patients who should not receive iodine-based CT contrast agents, whether due to history of iodine allergy, renal insufficiency, or renal transplantation. All of the U.S. Food and Drug Administration-approved gadolinium-based chelates used for MR imaging have very favorable safety profiles relative to the intravenous iodine-based agents used for CT. True anaphylactic reaction to gadolinium chelates is extremely rare, and these agents may safely be used in patients with very limited renal function.

Optimal renal imaging with CT or MR imaging generally requires multiphasic data acquisition following intravenous contrast administration. Although radiation dose has become an issue with multiphasic CT examination, particularly in evaluation of children and women of childbearing age (LOCKHART and SMITH 2003), MR imaging, of course, employs no ionizing radiation and therefore multiphasic post-contrast data acquisition does not confer additional risk to the patient.

E. S. PRETORIUS, MD
Wallace T. Miller Sr. Chair of Radiologic Education, Residency Program Training Director, MRI Section, Department of Radiology, University of Pennsylvania Medical Center, 1 Silverstein, 3400 Spruce Street, Philadelphia, PA 19104, USA

4.2 General Technical Considerations

Renal MR imaging examinations are best performed on high-field (1.0–1.5 T) systems, using a torso phased-array surface coil centered at the level of the kidneys to allow appropriately small fields of view (FOV) and to maximize the signal-to-noise ratio (SNR). A bellows may be placed around the patient's abdomen to permit the acquisition of respiratory-triggered images.

Use of low-field scanners for renal MR imaging examinations should, in general, be discouraged. Low-field scanners require very long imaging times to generate acceptable SNR, lack the gradient magnet speed and strength to acquire the thin slices required for adequate spatial resolution, and are incapable of imaging quickly enough to acquire truly dynamic post-contrast images. Although some patients and referring clinicians may specifically request the use of a low-field open scanner for a particular examination, it is incumbent upon the radiologist to fully disclose the limitations of renal MR imaging examinations performed on these systems.

Whole-body 3-T systems have recently become commercially available, and their role in renal MR imaging is likely to become prominent (ZHANG et al. 2003; NORRIS 2003). They offer twice the SNR of 1.5-T scanners, which may obviate the need for use of surface coils. Furthermore, the increase in SNR afforded by 3-T systems is likely to expand the role of parallel imaging for renal MR imaging, thereby dramatically decreasing imaging times (MCKENZIE et al. 2004). Parallel imaging techniques, and partial parallel imaging techniques such as sensitivity encoding (VAN DEN BRINK et al. 2003) and simultaneous acquisition of spatial harmonics (BYDDER et al. 2002), allow fast imaging sequences to be accelerated by utilizing spatial information inherent in the geometry of the surface-coil array to generate missing lines of k-space (HEIDEMANN et al. 2003). This effectively allows multiple lines of k-space to be generated for each phase-encoding step, decreasing imaging time; however, in parallel imaging, SNR decreases with increasing acceleration factor (LIN et al. 2004). A great advantage of 3-T scanners is that SNR lost to parallel imaging techniques could be compensated for by the higher SNR available at 3 T (due to increased spin polarization at the higher field strength), without compromising overall image quality. Limitations of 3-T renal imaging, however, include scanner cost and availability, as well as a probable increased incidence of severe

patient claustrophobia due to the architecture of these scanners.

Intravenous contrast material is best administered with an MR-compatible power injector, to provide reliable and reproducible delivery of the gadolinium chelate. No difference in efficacy has been demonstrated among the FDA-approved extracellular gadolinium chelate contrast materials: gadopentetate dimeglumine (Magnevist, Berlex Laboratories, Wayne, N.J.), gadodiamide (Omniscan, Nycomed Amersham Imaging, Princeton, N.J.), and gadoteridol (Prohance, Bracco Diagnostics, Princeton, N.J.). For renal imaging, all three of these agents may be administered at a dose of 0.2 ml/kg. An injection rate of 2 ml/s is used, and the contrast material injection is followed with a saline flush of 20 ml.

As circulation times vary greatly among patients, the use of a fixed-time delay to imaging is not recommended. This is particularly important in avoiding venous contamination of arterial-phase images for optimal renal MR angiography (MRA) examinations. The routine use of automated bolus detection (Smartprep, GE Medical Systems, Milwaukee, Wis.) or "fluoroscopic" monitoring (Carebolus, Siemens Medical Systems, Erlangen Germany) provides high-quality reproducible MRA examinations.

4.3 Goals of Oncologic Renal MR Imaging Examinations

The MR imaging examinations of potential renal malignancies should be tailored to determine whether or not a renal mass is present, and, if present, whether the mass is benign or malignant. The MR imaging examinations can be used to stage renal malignancies and can serve as a guide to appropriate choice of therapy. Finally, MR imaging has an important role to play in follow-up imaging of patients who have had nephrectomy, partial nephrectomy, or percutaneous tumor ablation.

4.3.1 Renal Lesion Detection

Improved radiologic detection of renal masses by US, CT, and MR imaging has led to smaller average size of neoplasm at time of initial detection (CURRY 2002), and most of these incidentally discovered renal cell carcinomas (RCC) are of low stage and

tumor grade (TSUI et al. 2000). In prior decades, nearly all patients with RCC presented with hematuria or other genitourinary symptomatology. Presently, however, approximately 30% of all RCCs are incidentally identified on imaging studies performed for other purposes (BONO and LOVISOLO 1997).

Computed tomography with thin-section (5 mm or thinner), pre- and post-contrast images can characterize most renal neoplasms larger than 1 cm. Many renal masses detected on CT, however, will be found on enhanced studies performed for non-renal indications where pre-contrast images were not performed. As such, many of these masses will not be adequately characterized, as the degree of renal enhancement cannot be assessed. Further evaluation with dedicated renal CT or MR imaging may be required.

The ability of dedicated renal CT and gadolinium-enhanced MR imaging to detect and characterize renal lesions greater than 1 cm is similar, although MR imaging is superior in the detection of small polar lesions due its ability to image directly in non-axial planes (ROFSKY and BOSNIAK 1997). Magnetic

resonance imaging is the examination of choice for the characterization of renal masses in patients with limited renal function (creatinine >2.0 mg/dl), severe allergy to iodinated contrast, or for masses not adequately characterized by other imaging modalities. Neither CT nor MR imaging has been shown to be accurate in characterizing solid lesions smaller than 1 cm, although well-performed MR imaging is clearly capable of characterizing many of these lesions.

4.3.2 Renal Lesion Characterization

The goal of renal lesion characterization by CT or MR imaging, therefore, is to separate surgical lesions (RCC, cystic renal cell carcinoma, oncocytoma) from non-surgical lesions (cyst, hemorrhagic cyst, angiomyolipoma (AML), pseudotumor; Fig. 4.1). Some benign lesions, such as AML with minimal fat or renal leiomyomas, have imaging appearances

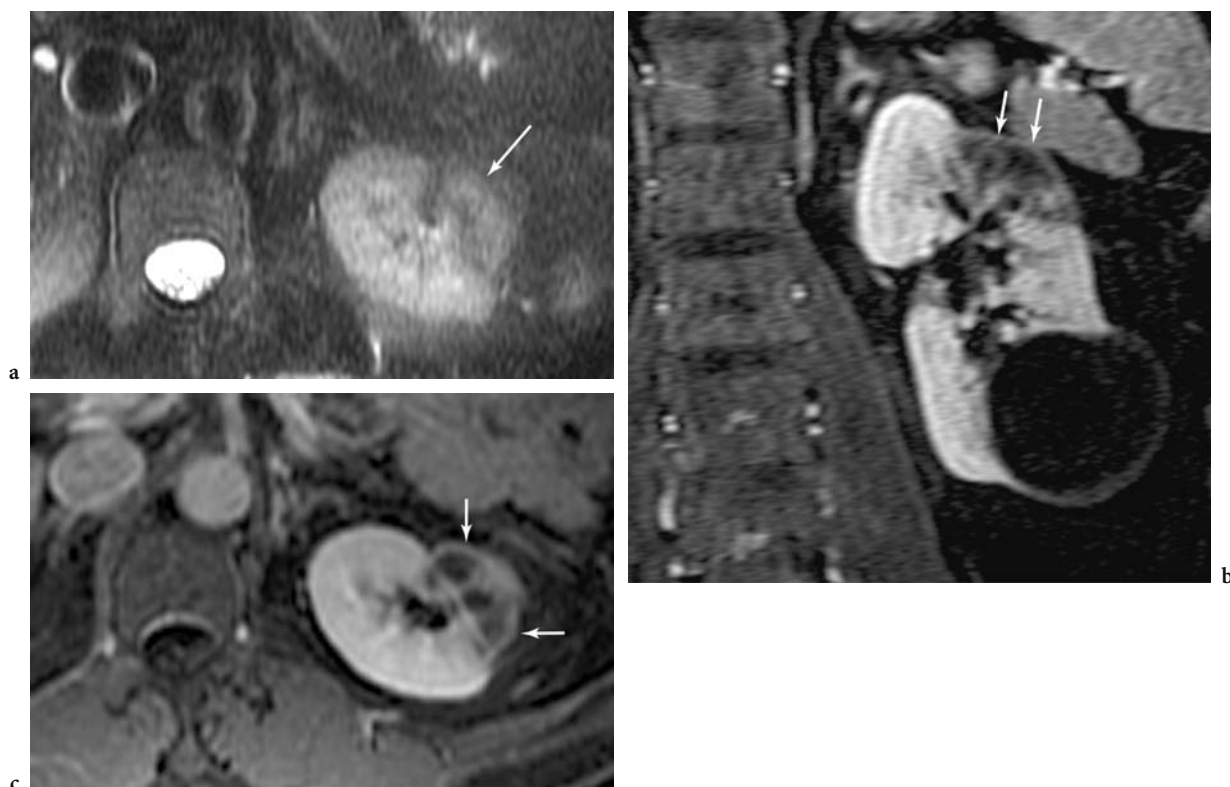


Fig. 4.1a-c. Flank pain and renal mass seen on US in a 46-year-old man. **a** Axial half-Fourier T2-weighted MR image (TR=not meaningful, TE=84 ms) demonstrates a possible mass (*arrow*) in the anterior interpolar region of the left kidney. **b** Coronal (TR=7.6 ms, TE=2.3 ms) and **c** axial (TR=195 ms, TE=1.4 ms) contrast-enhanced T1-weighted gradient-recalled-echo (GRE) MR images demonstrate very sharp, straight margins to the “mass,” indicating that this is a vascular insult. There is preservation of capsular blood flow (*arrows*) in this region of infarct, which was due to embolic disease.

which may be indistinguishable from RCC on any imaging modality (ISRAEL and BOSNIAK 2003b).

Renal cell carcinoma has a highly variable appearance on MR imaging, due to the existence of multiple RCC histologies (SHINMOTO et al. 1998), and to variability in internal necrosis, hemorrhage (JOHN et al. 1997), and/or intratumoral lipid. On MR imaging, RCC most commonly appears hypointense or isointense to renal parenchyma on T1-weighted images, heterogeneously hyperintense on T2-weighted images, and enhances following gadolinium administration. Variability is the rule, however, and lesions may be primarily hyperintense, hypointense, or isointense to normal renal parenchyma on both T1- and T2-weighted images. Although RCCs enhance with intravenous gadolinium administration, they tend to enhance less than normal renal parenchyma, and are often most easily identified on post-contrast dynamic T1-weighted gradient-recalled-echo (GRE) images (YAMASHITA et al. 1995).

Clear cell RCCs, the most common subtype of RCC, may lose signal on opposed-phase gradient-echo images, due to the presence of microscopic lipid in some of these neoplasms (Fig. 4.2; OUTWATER et al. 1997). The presence of intracellular lipid in a renal lesion should therefore not by itself be used to make the diagnosis of AML. The presence of macroscopic lipid (Fig. 4.3) within a renal lesion, however, remains very specific for AML, although very rare RCCs which have undergone osseous metaplasia may contain fat (HELENON et al. 1997).

Approximately 10–15% of renal cell carcinomas display some cystic component (HARTMAN et al. 1986). As with CT, the architectural features and enhancement characteristics of non-simple cystic renal lesions are important in determining lesion

management. The MR imaging features of cystic neoplasms that have been shown to be highly associated with malignancy include mural irregularity, mural nodules, increased mural thickness, and intense mural enhancement (BALCI et al. 1999).

Although the Bosniak classification system for cystic renal lesions was created for CT (BOSNIAK 1991), the morphologic features described in the various categories may be applied to MR imaging, with the limitation that calcifications are difficult to detect on MR imaging (ISRAEL and BOSNIAK 2004). Simple cysts are markedly T2 hyperintense, have a thin or imperceptible wall, display no internal architecture, and do not enhance (Fig. 4.4; NASCIMENTO et al. 2001). Lesions with a single thin septation or with fine mural calcification are probably benign (class II). Also in class II are small (<3 cm) CT “hyperdense” cysts, which contain internal protein or hemorrhage, and which therefore are hyperintense to normal renal parenchyma on T1-weighted images. These benign cysts do not enhance following contrast administration and have variable T2 signal intensity depending on their protein content. Subtraction imaging or direct region of interest (ROI) measurements on source images can be used to document lack of enhancement in these lesions. Cystic renal lesions with thicker septations, multiple septations or bulky calcifications are indeterminate, and should be excised (class III; Figs. 4.5, 4.6). Lesions with enhancing mural solid nodules (class IV) should be excised, and the majority of these lesions will be cystic RCCs (Fig. 4.7). Surgical cure rates for cystic RCC are very high (CORICA et al. 1999).

Category IIF lesions are lesions which are thought to be benign, but due to some internal complexity (number of internal septations, nodularity of calcification, T1-hyperintense cystic lesion >3 cm) require

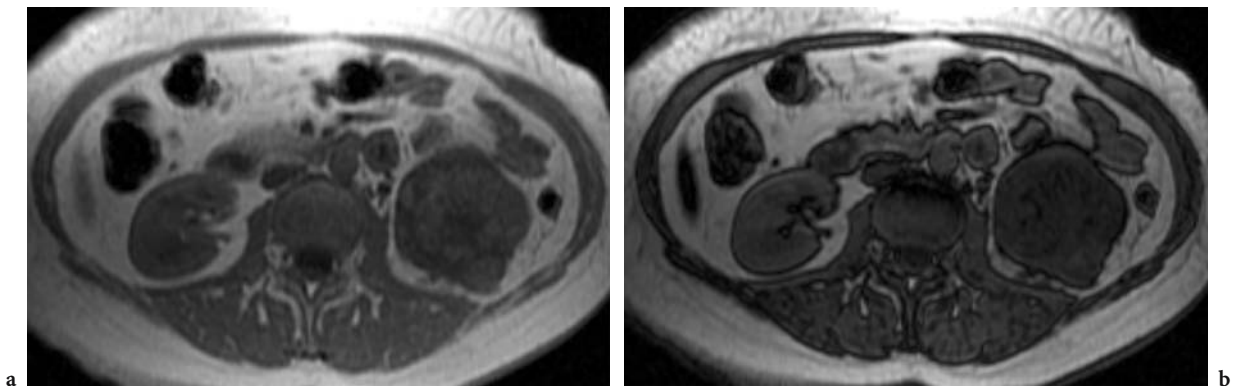


Fig. 4.2a,b. Hematuria and abdominal pain in a 54-year-old woman. Axial T1-weighted **a** in-phase (TR=185 ms, TE=4.2 ms) and **b** out-of-phase (TR=185 ms, TE=2.1 ms) GRE MR images demonstrate signal loss in this clear cell RCC of the left kidney due to the presence of intracytoplasmic lipid in the cells of the tumor.

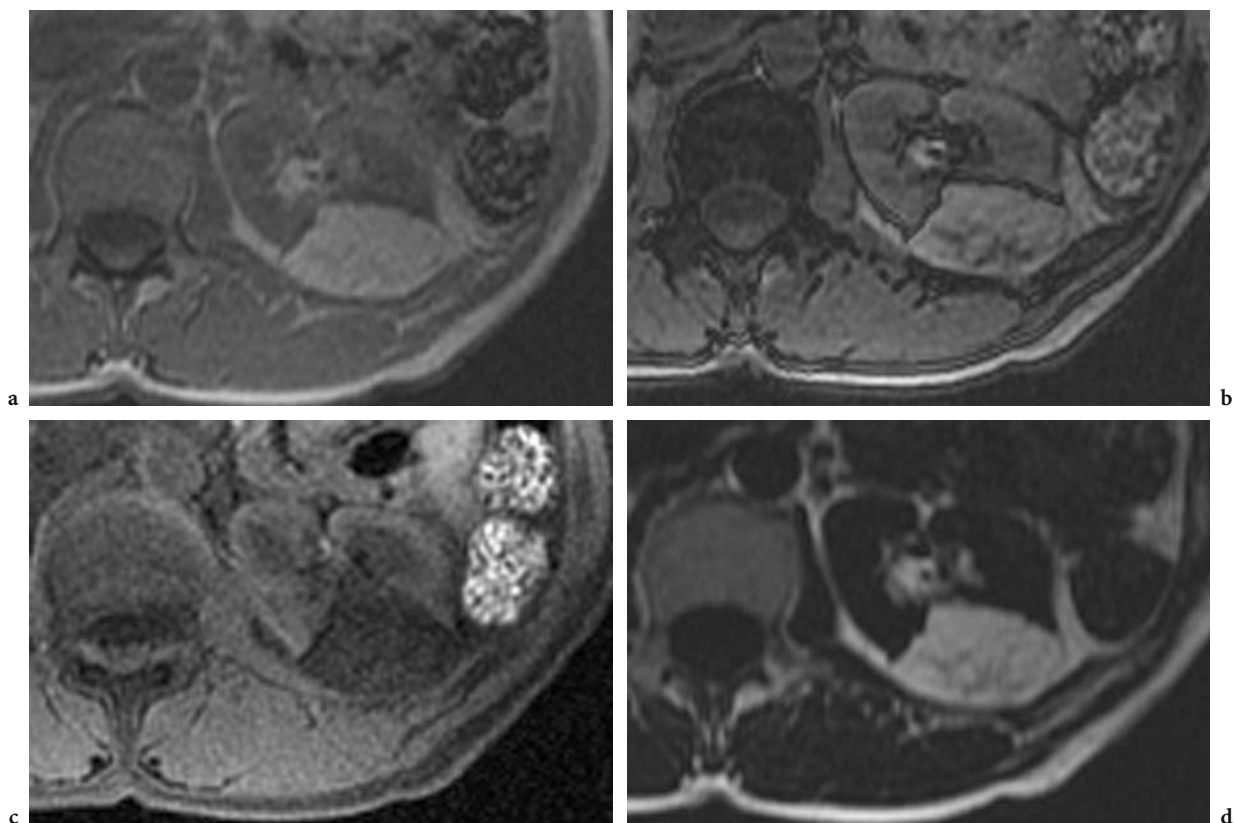


Fig. 4.3a-d. Renal angiomyolipoma in a 38-year-old woman. Axial T1-weighted gradient-echo MR images obtained **a** in phase (TR=275 ms, TE=4.6 ms), **b** out-of-phase (TR=275 ms, TE=2.3 ms), **c** with frequency-selective fat-suppression (TR=275 ms, TE=2.3 ms), and **d** with frequency-selective water saturation (TR=275 ms, TE=4.6 ms) demonstrate a benign left renal angiomyolipoma. Signal loss on the out-of-phase image relative to the in-phase image confirms the presence of both water and microscopic lipid. Signal intensity similar to that of the body wall fat on the fat-saturated and water-saturated images affirms the presence of macroscopic fat within the lesion, confirming the diagnosis of benign angiomyolipoma.

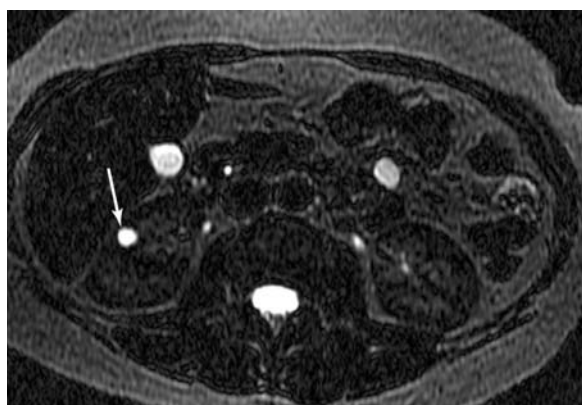


Fig. 4.4. Renal cyst in a 42-year-old woman. Axial heavily T2-weighted MR image (TR=not significant, TE=601 ms) demonstrates a thin-walled, fluid signal lesion (*arrow*) in the right kidney. This is a Bosniak I simple renal cyst.

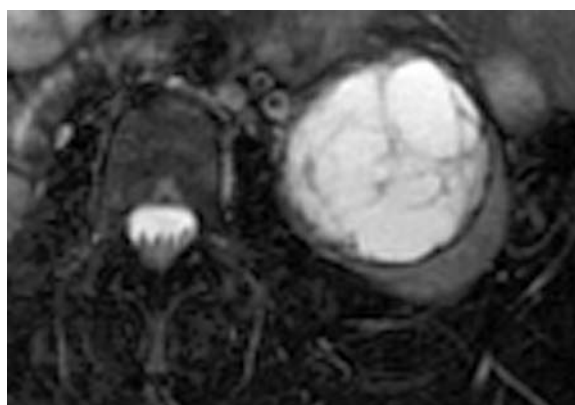


Fig. 4.5. Hematuria in a 42-year-old woman. Axial fat-suppressed respiratory-triggered fast-spin-echo T2-weighted MR image (TR=13043 ms, TE(eff)=120 ms) demonstrates a thickly septate, Bosniak III left renal lesion. This proved to be a cystic renal cell carcinoma.

follow-up at 6 and 12 months to determine stability (ISRAEL and BOSNIAK 2003a).

Most cystic neoplasms which require surgery will enhance greater than 20 Hounsfield units (HU) on CT, and enhancement of less than 12 HU is probably not significant in the absence of other lesion features suspicious for malignancy (SILVERMAN et al. 1994). Degree of CT enhancement is dependent on scanner software and calibration, and some helical-CT-ren-



Fig. 4.6. Incidentally discovered cystic renal mass on CT in a 66-year-old woman. Coronal contrast-enhanced T1-weighted GRE MR image (TR=3.8 ms, TE=0.8 ms) demonstrates a thick internal septation (*arrow*) in this lesion, making this a Bosniak III lesion. Excision was advised, and this was a cystic RCC.

dering algorithms may erroneously increase post-contrast CT attenuation values in simple cysts adjacent to dense excreted iodine (MAKI et al. 1999). The absence of an absolute scale of intensity in MR imaging makes it difficult to quantify degree of enhancement, although an ROI increase of greater than 15% (nephrographic phase at 2–4 min compared with pre-contrast) is suspicious for malignancy (Ho et al. 2002). Pre- and post-contrast MR images should always be obtained with identical imaging parameters, so that meaningful intensity comparisons can be made.

4.3.3

Staging of Renal Cell Carcinoma by MR Imaging

As RCC is relatively resistant to both radiotherapy and chemotherapy, surgical procedures have long been the mainstay of therapy (DEKERNION and MUKAME 1987). Accurate radiologic staging is critical in directing appropriate approach and resection for maximal disease control. Staging is also critical in determining prognosis, as tumor stage at time of diagnosis correlates directly with average survival. Renal cell carcinoma is most commonly staged using the Robson classification (ROBSON et al. 1969), although the TNM system may also be employed (Table 4.1; ERGEN et al. 2004).

Both CT and MR imaging have both been shown to be effective in staging RCC, with accuracies of approximately 90% reported for both modalities

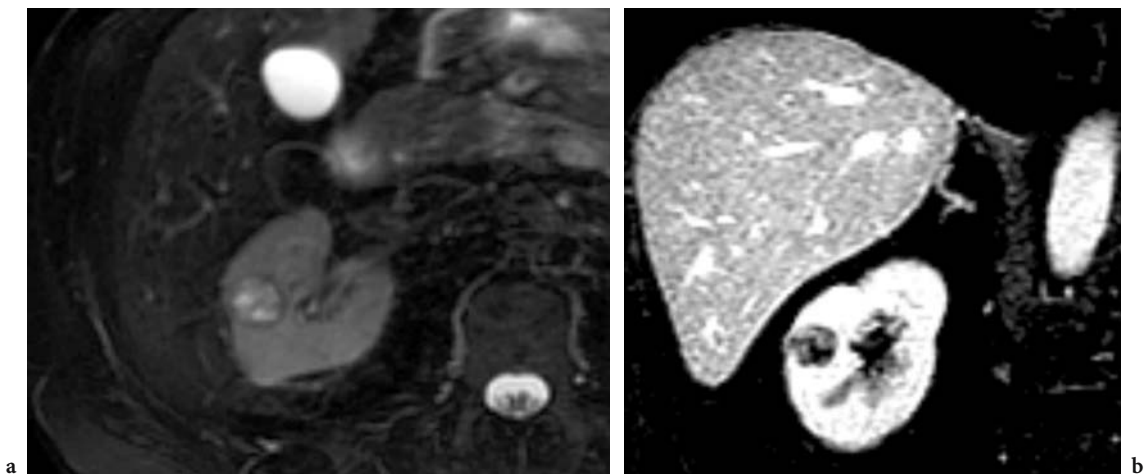


Fig. 4.7a,b. Hematuria in a 62-year-old man. **a** Axial fat-suppressed respiratory-triggered fast-spin-echo T2-weighted MR image (TR=12000 ms, TE=102 ms) demonstrates a cystic lesion with mural nodules in the right kidney. **b** Coronal 3D T1-weighted GRE MR image (TR=3.4 ms, TE=0.9 ms) demonstrates enhancement within the mural nodules. This is a Bosniak IV lesion, and was a cystic RCC.

Table 4.1. Staging of renal cell carcinoma

Robson stage	Description	TNM	TNM stage
I	Tumor confined to renal capsule		
	Small tumor (<2.5 cm)	T1	I
	Large tumor (>2.5 cm)	T2	II
II	Tumor spread to perinephric fat or adrenal	T3a	III
IIIA	Venous tumor thrombus		
	Renal vein thrombus only	T3b	III
	IVC thrombus	T3c	III
IIIB	Regional lymph node metastases	N1-N3	III/IV
IIIC	Venous tumor thrombus and regional nodes	T3b/c, N1-N3	III/IV
IVA	Direct invasion of adjacent organs outside Gerota's fascia	T4	IV
IVB	Distant metastases	M1	IV

(REZNEK 1996; ZAGORIA and BECHTOLD 1997). Magnetic resonance imaging appears to be superior for evaluation of tumor involvement of the perinephric fat, the renal vein, the inferior vena cava, and adjacent organs (PATEL et al. 1987). Ultrasound, although useful in screening for the presence of renal tumors, is limited in its ability to stage RCC because of difficulty in assessing retroperitoneal lymphadenopathy (BECHTOLD and ZAGORIA 1997). High accuracies for staging of advanced RCC have also been reported for fluorine-18 fluorodeoxyglucose (FDG) positron emission tomography (PET; RAMDAVE et al. 2001), although few such investigations have been performed.

Computed tomography cannot reliably differentiate Robson stage-I disease (tumor confined by the renal capsule) from Robson stage-II disease (tumor spread to the perinephric fat). This distinction has not historically been critical, as the perinephric fat would be routinely excised as part of a radical nephrectomy (CHOYKE 1997). If, however, partial nephrectomy is contemplated, it is desirable to know preoperatively if the perinephric fat is invaded by cancer, as this may affect the surgical approach (Fig. 4.8). One study has shown MR imaging to be slightly superior to CT in making this determination (FEIN et al 1987). In particular, the negative predictive value of MR imaging appears to be high; in one series, in 38 of 38 MR imaging cases (100%) in which the perinephric fat was thought to be uninvolved by tumor, this finding was confirmed at pathologic sectioning (Pretorius et al. 1999). This determination is best made on in-phase T1-weighted GRE images.

Fat-suppressed T2-weighted images are among the best MR images for detection of abdominal lymphadenopathy (Fig. 4.9). At present, MR imag-

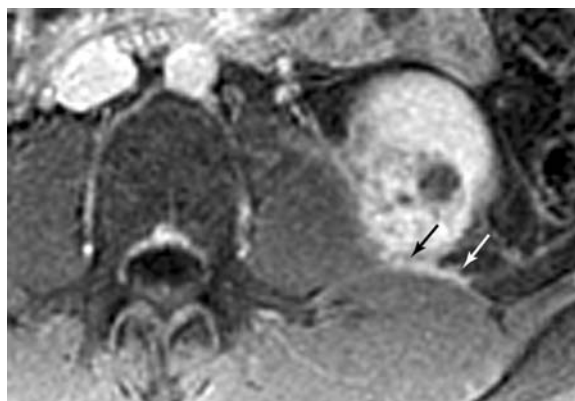


Fig. 4.8. Renal cell carcinoma invading perinephric fat in a 35-year-old man. Axial contrast-enhanced fat-suppressed gradient-echo T1-weighted MR image (TR=150 ms, TE=1.2 ms) demonstrates a left RCC. There is abnormal enhancement of the fat (arrows) posterior and medial to the kidney, adjacent to the left psoas muscle, representing tumor invasion of the perinephric fat.



Fig. 4.9. Stage-IV RCC in a 55-year-old man. Axial fat-suppressed respiratory-triggered fast-spin-echo T2-weighted MR image (TR=5516 ms, TE(eff)=94.7 ms) demonstrates a large left retrocrural node (long arrow) and a right basilar pulmonary metastasis (short arrow) at time of presentation.

ing is limited to anatomical imaging for evaluation of tumor spread to lymph nodes, although MR imaging with iron-based agents have shown promise in differentiating malignant from hyperplastic nodes (ANZAL et al. 2003). Contrast-enhanced 3D MR venography (MRV) images can detect renal vein and inferior vena cava (IVC) thrombus, and MR imaging's direct multiplanar imaging capabilities make it superior to CT in determining whether adjacent organs are directly invaded by the RCC (HRICAK et al. 1988).

4.3.4 Therapy Planning

Radical nephrectomy, which involves resection of the entire kidney, the proximal ureter, and ipsilateral adrenal gland, was for many years the sole surgical therapy offered to patients with RCC (ELGALLEY 2003). Recently, many studies have examined the efficacy of partial nephrectomy for select renal neoplasms, namely those that occur in solitary kidneys, synchronously in both kidneys, or in those patients with poor renal function. Reported rates of local tumor recurrence following radical nephrectomy are approximately 2% (ITANO et al. 2000). In one large series, local tumor recurrence from partial nephrectomy was approximately 3.2% (HAFEX et al. 1999), but overall patient survival has not differed significantly from that of patients with similar-stage disease who have undergone radical nephrectomy (D'ARMIENTO et al. 1997; LICHT et al. 1994; STEINBACH et al. 1995).

Many institutions now perform “elective” partial nephrectomy in patients with small renal neoplasms and normal contralateral kidneys, and studies have demonstrated no difference in patient 5- or 10-year survival (FERGANY et al. 2000; GHAVAMIAN and ZINCKE 2001) or in patient quality of life (CLARK et al. 2001). Open partial nephrectomy may carry a slightly lower surgical complication rate than radical nephrectomy, although both procedures have relatively low morbidity and mortality (CORMAN et al. 2000).

Imaging parameters which suggest that a renal lesion can be successfully and completely removed by partial nephrectomy include: small (<4 cm)

tumor size; peripheral location of the tumor; lack of invasion of the renal sinus fat, perinephric fat, and renal collecting system; presence of a pseudocapsule; lack of renal vein involvement; and absence of lymphadenopathy or distant metastases (PRETORIUS et al. 1999). Larger tumors and lesions that are locally invasive of the renal sinus fat (Fig. 4.10), renal collecting system, or perinephric fat may be removed by partial nephrectomy if there are compelling reasons (i.e., limited renal function, bilateral renal malignancies, or tumor in a solitary kidney). The presence of tumor thrombus or adjacent organ invasion excludes the possibility of a curative partial nephrectomy.

An evolving alternative to open surgery is laparoscopic partial nephrectomy (GUILLONNEAU et al. 2001). Although previously applied solely to benign disease, such as chronic pyelonephritis or calculus disease, the technique has now been advocated for use with small, indeterminate renal masses (HOLLENBECK and WOLF 2001). This is generally performed on lesions up to 2 cm and is associated with very low morbidity and mortality (JANETSCHKEK et al. 1998). Laparoscopic access has also been used for tumor cryoablation, radiofrequency (RF) ablation, focused ultrasound, and microwave therapy (EDMUNDS et al. 2000; MURPHY and GILL 2001; NAITO et al. 1998; YOSHIMURA et al. 2001). Although technical procedural success has been reported, it remains to be seen whether these new therapies will match the high tumor cure rates achieved by open radical and partial nephrectomies (RASSWEILER et al. 2000).

Some institutions have performed MR-guided interventions on low-field, open MR imaging scan-

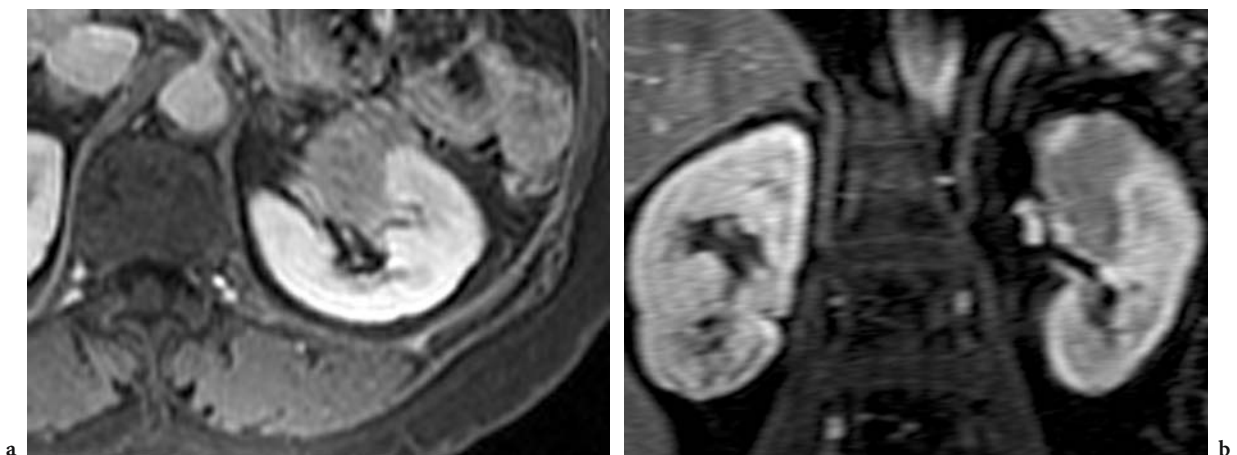


Fig. 4.10a,b. Renal mass in a 63-year-old woman with history of non-Hodgkin lymphoma. **a** Axial contrast-enhanced 2D T1-weighted GRE (TR=200 ms, TE=1.4 ms) and **b** coronal contrast-enhanced 3D T1-weighted GRE (TR=7.7 ms, TE=2.4 ms) MR images demonstrate a rounded mass of the left upper renal pole extending into the renal sinus fat. This was a renal recurrence of the patient's B-cell non-Hodgkin lymphoma.

ners (LEWIN et al. 1998; SEWELL et al. 2003), although CT guidance is more commonly used (HINSHAW and LEE 2004; ZAGORIA 2003). Among the advantages of combining real-time MR imaging with focused tumor ablation are the ability to confirm the presence of the RF electrode or cryoablation device within the tumor, and the ability to perform high-resolution, real-time imaging to confirm adequate tumor treatment. As availability of such open interventional scanners increases and image quality improves, the frequency of such procedures is likely to increase.

4.3.5 Post-Therapy Imaging

Authors differ in recommendations for imaging follow-up after surgical treatment for RCC, although recurrence rates are known to be related to the size, histologic grade, and stage of the primary neoplasm (BLUTE et al. 2000). In one retrospective study of 200 patients with RCC treated with radical or partial nephrectomy (Fig. 4.11), no patient with T1 neoplasm smaller than 4 cm had tumor recurrence at mean follow-up 47 months (GOFRIT et al. 2001), so patients with such tumors may not need routine imaging follow-up. Patients with larger tumors, high tumor grade, or advanced stage may be followed with semi-annual chest CT and with abdominal CT (GOFRIT et al. 2001) or MR imaging. Local tumor recurrence following complete resection is relatively rare (<2% at 5 years), but it carries a poor prognosis, with 28% survival at 5 years (Figs. 4.12, 4.13; ITANO et al. 2000).

Few studies have been performed on imaging following focal laparoscopic ablation of renal neoplasms. The MR imaging appearance of post-cryoablation has been reported, and most cryoablated lesions (95%) were isointense to hypointense to normal parenchyma on T2-weighted images, and a minority of lesions displayed a thin T2 hypointense rim. Serial imaging demonstrates interval decrease in size of the cryoablation site (REMER et al. 2000). The utility of MR imaging as follow-up imaging for RF ablation of solid renal tumors has also been established (Fig. 4.14; FARRELL et al. 2003).



Fig. 4.12. Tumor recurrence in a 50-year-old man post-right nephrectomy. Coronal contrast-enhanced T1-weighted GRE MR image (TR=7 ms, TE=2.2 ms) demonstrates avidly enhancing nodal recurrence (*arrow*) posterior to the inferior vena cava.

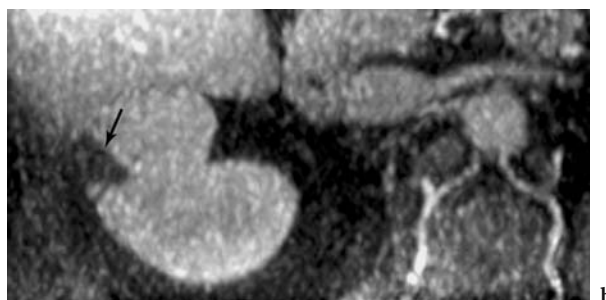
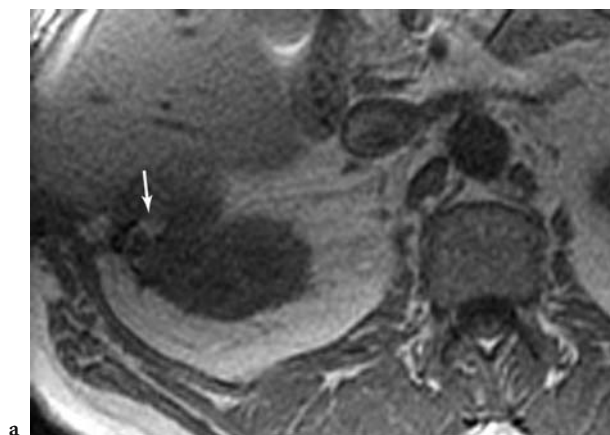


Fig. 4.11a,b. Follow-up MR imaging in a 62-year-old man with history of partial nephrectomy. Axial a in-phase (TR=160 ms, TE=4.7 ms) and b contrast-enhanced (TR=140 ms, TE=1.3 ms) T1-weighted GRE MR images demonstrate fat signal in the patient's partial nephrectomy defect (*arrow*). This is a common appearance, as fat is often used to fill the defect created by wedge resection.

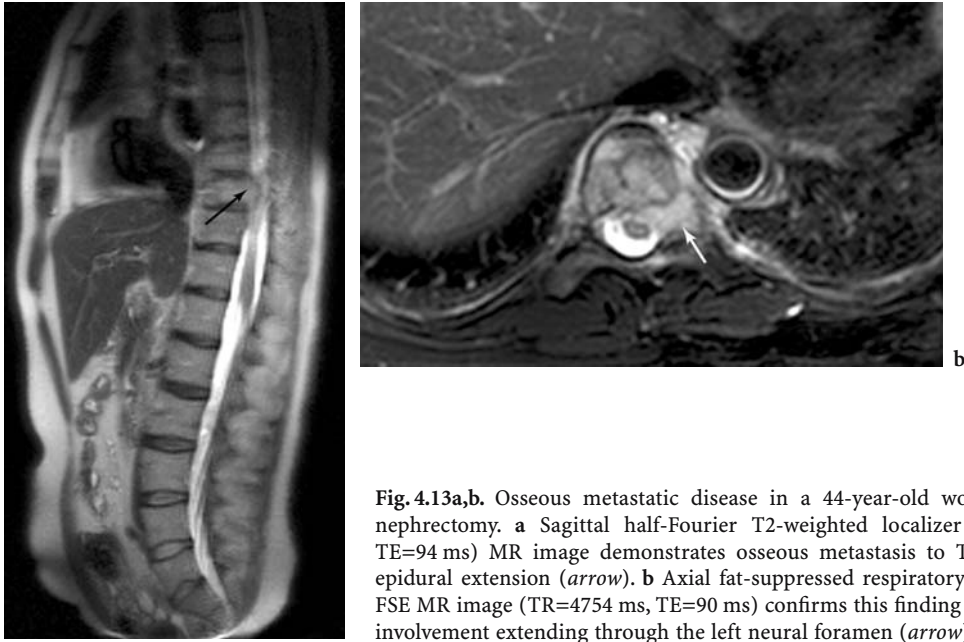
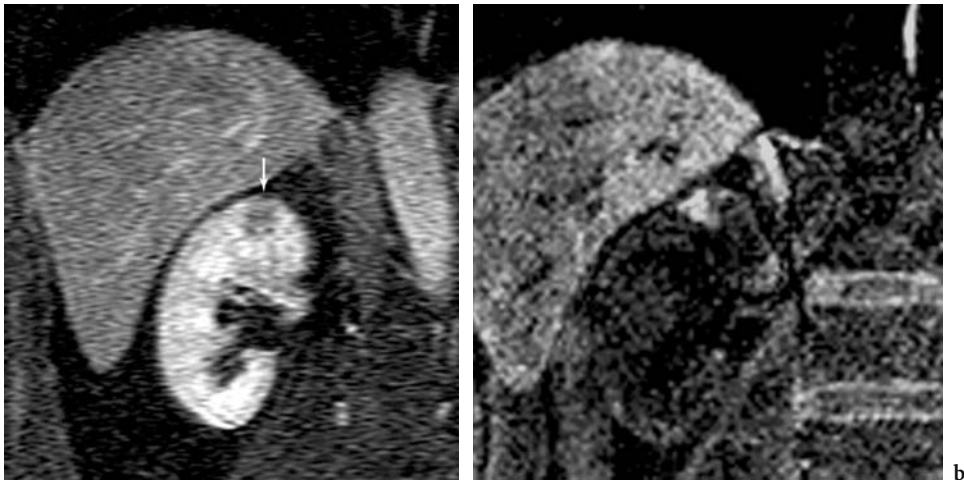
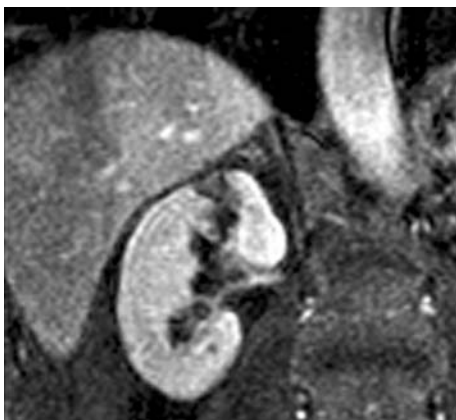


Fig. 4.13a,b. Osseous metastatic disease in a 44-year-old woman following partial nephrectomy. **a** Sagittal half-Fourier T2-weighted localizer (TR=not meaningful, TE=94 ms) MR image demonstrates osseous metastasis to T9 vertebral body with epidural extension (*arrow*). **b** Axial fat-suppressed respiratory triggered T2-weighted FSE MR image (TR=4754 ms, TE=90 ms) confirms this finding and shows the epidural involvement extending through the left neural foramen (*arrow*).



a

b



c

Fig. 4.14a-c. Renal cell carcinoma in a 56-year-old man before and after radiofrequency ablation. **a** Coronal pre-ablation contrast-enhanced T1-weighted GRE MR image (TR=4.5 ms, TE=2.0 ms) demonstrates enhancing solid RCC (*arrow*) of right upper renal pole. **b** Coronal post-ablation unenhanced T1-weighted GRE MR image (TR=4.7 ms, TE=1.8 ms) demonstrates hyperintensity in the region of ablation, representing hemorrhage. **c** Coronal post-ablation contrast-enhanced T1-weighted GRE (TR=4.7 ms, TE=1.8 ms) demonstrates no enhancement in this area, which was confirmed with region-of-interest placements. The absence of enhancing tissue confirms successful ablation.

4.4 Suggested MR Imaging Protocol

A suggested protocol for MR imaging of a potential renal mass is presented in Table 4.2.

4.4.1 Localizer Images

Localization may be performed in a breath-hold, with either a multiplanar 2D T1-weighted GRE sequence or with a half-Fourier single-shot T2-weighted sequence (Fig. 4.15). Either of these sequences can fulfill the purpose of localization, allowing selection of an appropriate center and field of view for the remainder of the examination. As the localizer sequence has the largest field of view of any sequence performed, however, there are some anatomic areas that are visualized on the localizer sequence only. As such, the T2-weighted sequence (single-shot fast spin echo (SSFSE), GE Medical Systems; half-Fourier acquisition single-shot turbo spin echo (HASTE), Siemens Medical Solutions) is preferred due to the superior tissue contrast of T2-weighted images. This allows characterization of pleural or pericardial effusions, as well as many findings in the bowel, bones, and pelvis.

It is not uncommon that the localizer sequence alone provide diagnostic information or reveal findings (e.g., solitary kidney, widespread metastatic disease) that may require modification of a standard renal protocol.

4.4.2 T1-Weighted Images

Chemical shift imaging with 2D, multishot in-phase and opposed-phase spoiled T1-weighted GRE images should be part of all abdominal MR imaging examinations (fast spoiled gradient-recalled (FSPGR), GE

Medical Systems; fast low-angle shot (FLASH), Siemens Medical Solutions). If fat and water are present in the same voxel, loss of signal will be seen on the opposed-phase image relative to the in-phase images due to destructive interference of the fat and water signals. These sequences are used to detect the presence of intracytoplasmic lipid in hepatic steatosis, hepatic adenomas, hepatocellular carcinomas, and adrenal adenomas (OUTWATER et al. 1998). In the kidney, signal loss on chemical shift imaging is not specific for angiomyolipoma, as clear cell RCC may also contain intracytoplasmic lipid (Fig. 4.2; OUTWATER et al. 1998).

The TR of these 2D T1-weighted GRE images is adjusted based on the patient's ability to breath-hold, as it is desirable to image the entire kidney in a single breath-hold. At 1.5 T, the TE of the in-phase image will be 4.4 ms and the TE of the directly

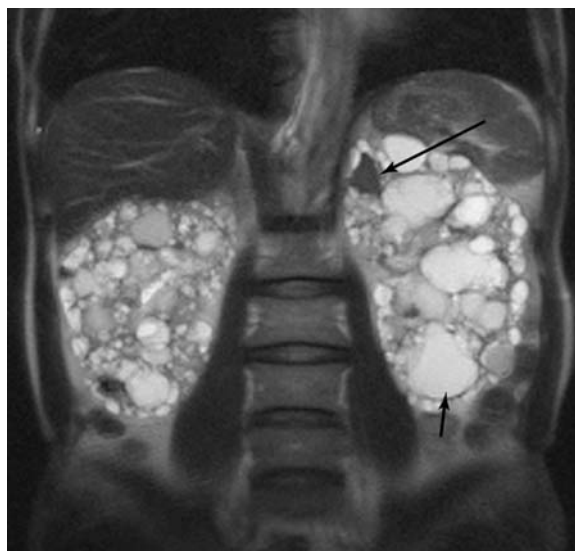


Fig. 4.15. Autosomal-dominant polycystic kidney disease in a 45-year-old man. Coronal half-Fourier T2-weighted localizer MR image (TR=not meaningful, TE=86 ms) reveals multiple simple (*short arrow*) and hemorrhagic (*long arrow*) cysts within greatly enlarged kidneys.

Table 4.2. Suggested protocol: renal mass on 1.5 T MR scanner. FOV field of view; NA not applicable

	Sequence	Plane	TR (ms)	TE (ms)	Flip angle (°)	FOV (cm)	Thickness (mm)	Skip (mm)
Localizer	T2 half-Fourier	Coronal/sagittal	NA	80–100	NA	40–48	8	2
Chemical shift	T1-GRE (in phase)	Axial	120–200	4.4	90	26–38	6	1
Chemical shift	T1-GRE (out of phase)	Axial	120–200	2.2	90	26–38	6	1
Respiratory triggered fat-suppressed T2	T2 FSE	Axial	4000–12,000	80–110 (eff)	NA	26–38	7	1
Pre/post-contrast 3D	T1-GRE	Coronal	Minimum	Minimum	15	34	4 interpo- lated to 2	0
Delayed/post-contrast	T1-GRE	Axial	120–280	1.1–1.4	90	26–38	6	1

opposed phase image will be 2.2 ms. The software of some manufacturers employs sequences that are slightly off these values, but which nonetheless are capable of detecting signal loss on the opposed-phase image when fat and water protons are present in the same voxel. These sequences can be obtained simultaneously in a single breath-hold by acquiring two echoes per excitation and reconstructing the data as separate series. This technique is preferable to acquisition in two breath-holds, because it eliminates respiratory misregistration between the two sequences.

Renal angiomyolipomas are benign hamartomas which are composed of varying amounts of blood vessels, smooth muscle, and fat. They are common in patients with tuberous sclerosis (CASPER et al. 2002) but may also occur sporadically. As they are vascular lesions, AMLs may enhance avidly on CT and MR imaging and must be differentiated from RCCs. Angiomyolipomas may contain both intracytoplasmic lipid – detectable with chemical shift imaging – and macroscopic fat, which can be confirmed with use of frequency-selective fat-suppressed T1-weighted GRE and water-saturated T1-weighted GRE images (Fig. 4.3; Table 4.3). These are both breath-held sequences, and should be obtained while maintaining the TR of the original in-phase and opposed-phase T1-weighted GRE sequences. These sequences allow definitive detection and characterization of the macroscopic fat present in most angiomyolipomas. If present, macroscopic fat will follow the signal of the perinephric fat and the body-wall fat, becoming hypointense to renal parenchyma on the fat-suppressed T1-weighted GRE and remaining very hyperintense on the water-saturated T1-weighted GRE.

Some AMLs do not contain macroscopic fat. At present, these lesions cannot be reliably differentiated from RCC by diagnostic imaging (HOSOKAWA et al. 2002; JINZAKI et al. 1997). The renal leiomyoma, a rare benign lesion, is thought to represent an angiomyolipoma devoid of fat due to the increased incidence of leiomyomas in patients with tuberous sclerosis (STEINER et al. 1990; WAGNER et al. 1997).

For patients who cannot breath-hold, respiratory-triggered FSE T1-weighted imaging is an option for obtaining pre-contrast T1-weighted images. This

technique is slower than T1-weighted GRE chemical shift imaging and provides less information, as the presence of microscopic lipid cannot be confirmed. This technique, therefore, is best reserved for sedated or ventilated patients.

4.4.3 T2-Weighted Images

For T2-weighted imaging, axial, fat-suppressed, respiratory-triggered FSE T2-weighted images offer excellent SNR and reasonable acquisition times. The FSE/TSE imaging is faster than conventional spin-echo imaging in that multiple-phase encodes are achieved in a single TR. The effective echo time of the sequence is determined by the TE of the phase encodes of the center of k-space, and this data dominates image contrast. Fat suppression is commonly applied to these sequences, as echo-train imaging results in higher signal intensity of fat than is routinely seen on conventional spin-echo T2-weighted images.

With respiratory triggering a bellows is placed around the patient's abdomen to monitor patient respiration. Acquisition of MR imaging data is performed at a fixed point in the respiratory cycle, minimizing respiratory-associated phase ghost artifacts. Although these images are generally excellent in quality, a detriment of this technique is that data can be collected in only a portion of the respiratory cycle, leading to relatively longer imaging times.

A promising alternative to respiratory triggering is navigator echo gating. This technique has been applied more in cardiac MR imaging than in abdominal imaging, but its potential for minimizing respiratory motion is well established (SODICKSON 2002). In navigator echo gating, targeted scans are used to establish the position of some anatomic object, such as the diaphragm, whose relationship to the organ of interest is predictable. Prior to each data acquisition, navigator echoes are generated by selectively exciting a column of tissue that traverses a high-contrast tissue interface, such as lung–diaphragm. Signal from this excitation is compared to a reference echo to establish the relative displacement of the navigator interface, and this data is used for

Table 4.3. Additional sequences: suspected angiomyolipoma on 1.5 T MR scanner

	Sequence	Plane	TR (ms)	TE (ms)	Flip angle (°)	FOV (cm)	Thickness (mm)	Skip (mm)
Fat suppression	T1-GRE	Axial	120–200	2.2	90	26–38	6	1
Water saturation	T1-GRE	Axial	120–200	4.4	90	26–38	6	1

respiratory gating of data acquired of the object of interest (FIRMIN and KEEGAN 2002). On most scanners, however, navigator echo gating is more challenging to optimize than respiratory triggering, and this has likely limited its use in routine imaging of the abdomen.

Although half-Fourier single-shot T2-weighted images (SSFSE, GE Medical Systems; HASTE, Siemens Medical Solutions) are adequate as localizer images, their SNR and contrast-to-noise ratio (CNR) relative to FSE/TSE T2-weighted images is too low to justify their routine use as the sole T2-weighted sequence of high-quality abdominal MR imaging. In half-Fourier imaging, just over one half of k-space is acquired in a single echo train, and k-space symmetry is used to infer the remainder of the non-acquired data. The result is a rapidly acquired image of low spatial resolution and relatively low contrast, which may render small or nearly T2-isointense renal malignancies undetectable (Fig. 4.16).

Half-Fourier imaging should not be the sole T2-weighted imaging sequence of a renal MR imaging examination; however, these sequences may serve as a useful adjunct to FSE/TSE T2-weighted images when employed as MR hydrography to evaluate the urothelium of a hydronephrotic, non-functioning kidney.

4.4.4 Pre- and Post-Contrast Imaging

The contrast-enhanced portion of the examination may be performed either as a 2D (FSPGR, GE Medical Systems; FLASH, Siemens Medical Solutions) or 3D (enhanced fast gradient-recalled echo (EFGRE), GE Medical Systems; volumetric interpolated breath-hold examination (VIBE), Siemens Medical Solutions) sequence (HEISS et al. 2000; ROFSKY et al. 1999). Three-dimensional images are greatly preferred, as they provide thinner sections, have no interscan gaps, suffer fewer partial-volume artifacts in evaluation of small lesions, and provide superior spatial resolution in the interpolated plane. The choice of 3D dynamic imaging allows renal MRA/MRV imaging to be performed at the same time that dynamically enhanced renal parenchyma data is acquired, although this commonly used approach requires some imaging compromises to be made. When primarily evaluating the renal parenchyma, a flip angle of 10–15° is used to minimize soft tissue saturation and optimize renal mass detection and characterization. If the study is for renal vascular evaluation, the flip angle is increased to 30–60° to optimize the contrast between enhanced vessels and

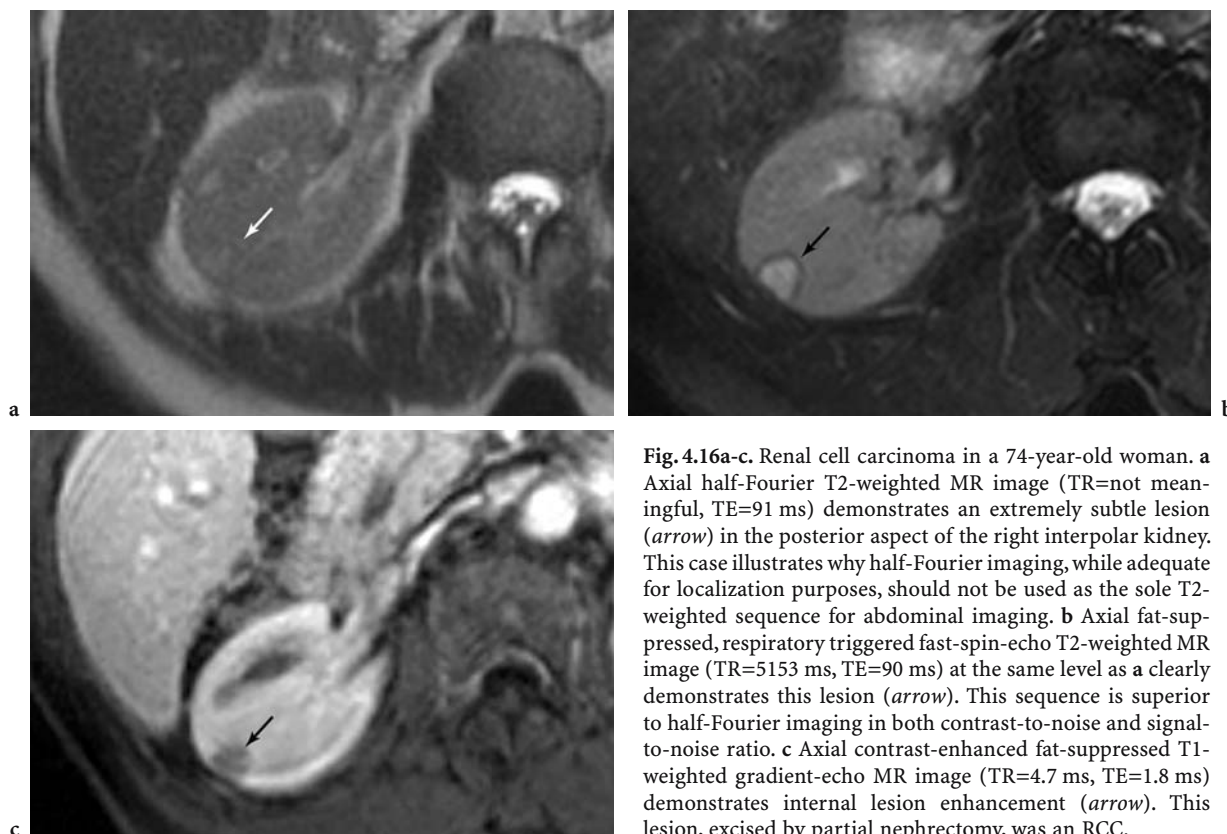


Fig. 4.16a-c. Renal cell carcinoma in a 74-year-old woman. **a** Axial half-Fourier T2-weighted MR image (TR=not meaningful, TE=91 ms) demonstrates an extremely subtle lesion (*arrow*) in the posterior aspect of the right interpolar kidney. This case illustrates why half-Fourier imaging, while adequate for localization purposes, should not be used as the sole T2-weighted sequence for abdominal imaging. **b** Axial fat-suppressed, respiratory triggered fast-spin-echo T2-weighted MR image (TR=5153 ms, TE=90 ms) at the same level as **a** clearly demonstrates this lesion (*arrow*). This sequence is superior to half-Fourier imaging in both contrast-to-noise and signal-to-noise ratio. **c** Axial contrast-enhanced fat-suppressed T1-weighted gradient-echo MR image (TR=4.7 ms, TE=1.8 ms) demonstrates internal lesion enhancement (*arrow*). This lesion, excised by partial nephrectomy, was an RCC.

the less-enhanced non-vascular soft tissues (ROFSKY et al. 1999). Field of view is also reduced in dedicated MRA examination, to increase spatial resolution.

For any contrast-enhanced MR imaging examination, a pre-contrast data set must be acquired. Its acquisition parameters must be identical to those of the post-contrast data sets so that potential lesion enhancement can be assessed. For renal parenchymal evaluation, images are acquired in both a corticomedullary phase and in a nephrographic phase. If the renal imaging is primarily for renal vascular evaluation, a renal arterial vascular phase may also be obtained, although use of a bolus timing technique is required to reliably capture this brief phase.

The coronal plane is generally chosen for the gadolinium-enhanced images as it allows dynamic evaluation of both kidneys, the renal vessels, and the inferior vena cava in the smallest number of slices or slabs. In general, though, for characterization of a known renal mass, one should choose the plane which best displays the mass. For exophytic anterior and posterior lesions, this may be the sagittal or axial plane. If the coronal plane is chosen, however, the patient's arms are elevated above the head to decrease phase-wrap artifact.

As dynamic 3D imaging of the kidneys necessarily may exclude portions of the liver, spleen, and other abdominal viscera to acquire the image within a reasonably short breath-hold, axial 2D delayed fat-saturated T1-weighted GRE images are obtained as the final sequence, imaging from the top of the hemidiaphragms to the iliac crests. This sequence provides full coverage of the contrast-enhanced abdominal viscera.

4.4.5

Subtraction Imaging

Subtraction imaging is a useful post-processing tool for interpretation of renal MR imaging. In subtraction imaging, each voxel of the pre-contrast data set is subtracted from a post-contrast data set. This may be performed by the technologist on the MR scanner, or by the radiologist on a workstation. Subtraction may be used to detect subtle enhancement in renal lesions (pre-contrast data set subtracted from nephrographic-phase data set); to improve the contrast-to-background ratio of MRA images (pre-contrast subtracted from arterial-phase data set); or to differentiate non-enhancing bland thrombus from enhancing tumor thrombus (precontrast subtracted

from MRV data set). One limitation of subtraction is respiratory misregistration between the pre-contrast and post-contrast data sets. This may result in "pseudoenhancement" of a renal lesion (Fig. 4.17). The presence of misregistration is identified by identifying a rim of hyperintensity around the kidneys and liver on the subtraction data set. If misregistration is severe, direct signal intensity measurements of the lesion in question on the pre- and post-contrast images must be performed to determine whether enhancement has occurred.

4.4.6

Functional Renal MR Imaging

Dynamic, multiphase contrast-enhanced MR imaging can also be used as a form of functional renal imaging (HUANG et al. 2003; HUANG et al. 2004; TEH et al. 2003). This technique has been applied for quantification of renal cortical enhancement in patients with renal artery stenosis (GANDY et al. 2003), and in assessment of enhancement in RCC (CHOYKE et al. 2003). As tumor angiogenesis has become a recognized feature of renal and other malignancies, contrast-enhanced MR imaging has emerged as a modality capable of demonstrating tumor neovascularity, quantifying contrast agent wash-in/wash-out curves, and evaluating the effects of antiangiogenic therapies (which may not produce changes in lesion size; HAYES et al. 2002). Examinations tailored for functional MR imaging of renal cell carcinoma typically use slower injection rates (0.3 ml/s of 0.1 ml/kg gadolinium chelate) and 3D T1-weighted GRE imaging of the kidney is performed approximately every 30 s for 8–10 min.

4.4.7

MR Angiography

Three-dimensional arterial and venous-phase 3D data sets are post-processed to generate projection images of the renal arteries, renal veins, and inferior vena cava. As 3D volumetric sequences result in small, nearly isotropic voxels, maximum intensity projection (MIP) images of the renal arteries, renal veins, and inferior vena cava (IVC) may be generated in any plane. Axial and coronal projections are most commonly used, but oblique coronal or curved reformatted images are often optimal for display of renal vessel anatomy. Volume rendering of renal vessels may also be used.

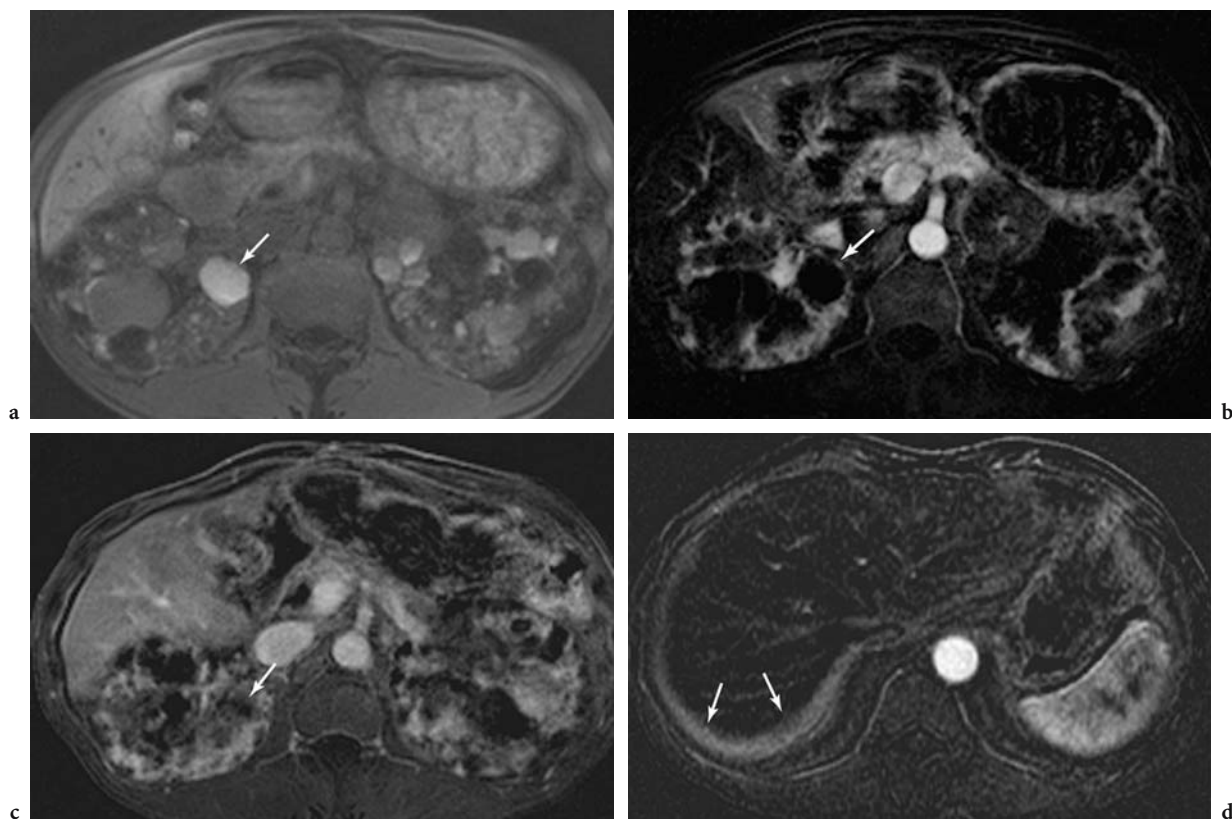


Fig. 4.17a-d. Autosomal-dominant polycystic kidney disease in a 45-year-old man. **a** Axial unenhanced fat-suppressed T1-weighted gradient-echo MR image (TR=3.8 ms, TE=0.9 ms) reveals many of the cysts to be hemorrhagic, including a large right posterior inter-polar hemorrhagic cyst (*arrow*). As such, it can be difficult to determine if any of the cysts have internal enhancement. **b** Axial subtraction MR image reveals no internal enhancement in any of the cystic lesions. The right posterior inter-polar lesion (*arrow*), in particular, does not enhance and is therefore a Bosniak II benign hemorrhagic cyst. **c** Axial subtraction image generated from a later contrast-enhanced acquisition. If contrast-enhanced images and unenhanced images are poorly registered due to differential breath-hold size, apparent enhancement in benign lesions (*arrow*) can result. **d** A more cranial axial MR image from the data set in **c** reveals a concentric bright band of misregistered enhancing tissue (*arrows*) around the liver. This confirms that this particular data set is poorly registered.

In MRA the order in which k-space is filled is an important consideration. Optimally, the central k-space data, which dominates the contrast of the image, should be acquired during the very brief time that gadolinium concentration is high in the renal arteries yet low in the renal veins. Use of a bolus timing technique is, of course, mandatory, but use of an elliptic-centric method of filling k-space (rather than traditional sequential filling) can effectively compress the time in which the critical central portion of k-space is filled (FAIN et al. 2001; WILMAN and RIEDERER 1997). This approach can be used to maximize contrast between the contrast-enhanced arteries and background.

The MRA/MRV constitutes an important part of the overall MR imaging evaluation of a renal malignancy, as several questions related to tumor staging and treatment strategy must be addressed (KOCÁK

et al. 2001). The number and position of renal arteries, the number and morphology of renal veins, the presence/absence of tumor thrombus in the renal vein and IVC, and the status of the vasculature of the contralateral kidney should all be evaluated.

Magnetic resonance angiography has emerged as a powerful modality for imaging the renal arteries (DONG et al. 1999; FAIN et al. 2001; ZHANG and PRINCE 2004). Compared with conventional angiography, which is the traditional gold standard diagnostic examination, MRA is considerably less invasive and has the additional advantage of utilizing a non-nephrotoxic contrast agent that can be administered safely in patients with elevated creatinine. Both MRA and CT angiography (CTA) have been reported to be 100% sensitive for the detection of main renal arteries (HALPERN et al. 2000; RANKIN et al. 2001). Accessory renal arteries are common,

however, occurring in approximately 29% of kidneys, and must be detected to allow proper surgical planning for radical nephrectomy (Fig. 4.18; NELSON et al. 1999).

Although early papers reported MRA to be inferior to conventional angiography for detection of accessory renal arteries (DEBATIN et al. 1993; MEYERS et al. 1995), MRA protocols have advanced (CARROLL and GRIST 2002) so that more recent investigations have found conventional angiography and dynamic, contrast-enhanced 3D MRA to be comparable (BUZZAS et al. 1997; Low et al. 1998).

Computed tomography angiography and MRA are approximately equal in their ability to demonstrate accessory renal arteries, with sensitivities of greater than 90% reported for both modalities (RANKIN et al. 2001). Smaller (1–2 mm) accessory renal arteries are subject to higher rates of non-detection by imaging, as well as greater likelihood of interobserver disagreement. Both CTA and MRA examinations of renal donors have demonstrated high degrees of interobserver agreement for presence of accessory renal arteries and for the presence of early arterial bifurcations (HALPERN et al. 2000).

4.4.8

MR Venography

Although tumor thrombus may be suspected on conventional T1- and T2-weighted images, 3D contrast-enhanced sequences can be used to confirm the presence of renal vein or IVC thrombus (CHOYKE et al. 1997). Venous phase enhanced MR images have been reported to be 88–100% sensitive in detection of malignant tumor renal vein thrombus (CHOYKE et al. 1997; LAISSY et al. 2000). In the renal donor population, MRV has been shown to be superior to digital subtraction angiography in characterizing renal venous anatomy (GIESSING et al. 2003).

Renal cell carcinoma involves the IVC in 5–10% of cases (KEARNEY et al. 1981). In evaluation of the IVC, the second or third set of contrast-enhanced coronal images is ideal for detection and characterization of the extent of thrombus within the renal veins and IVC. Generally, tumor thrombus enhances while bland thrombus does not (Figs. 4.19, 4.20, 4.21; EILENBERG et al. 1990; NGUYEN et al. 1996); however, both types of thrombus are removed at time of surgery.

The sensitivity of MR imaging has been reported to be 90–100% for detection of IVC thrombus, which is superior to rates reported for CT (79%) and sonog-

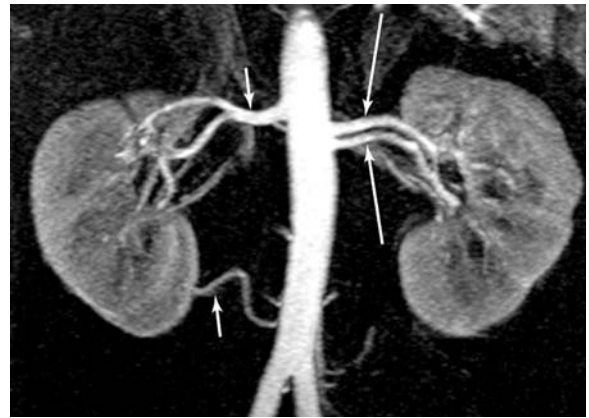


Fig. 4.18. Bilateral accessory renal arteries in a 47-year-old man. Maximum intensity projection (MIP) reformatted MR image of bolus-timed, arterial phase 3D T1-weighted GRE imaging of the kidneys (TR=3.8 ms, TE=0.9 ms) demonstrates two left renal arteries (*long arrows*) and two right renal arteries (*short arrows*).



Fig. 4.19. Renal cell carcinoma in a 47-year-old woman. Coronal subtracted maximum intensity projection (MIP) image of contrast-enhanced MRV examination (TR=3.7 ms, TE=1.4 ms) demonstrates bland, non-enhancing, non-occlusive thrombus of the inferior vena cava and left common iliac vein (*arrows*). There is a large right-upper-pole-enhancing RCC (*arrowheads*).

raphy (68%; KALLMAN et al. 1992; ASLAM SOHAIB et al. 2002). The CT specificity for detection of IVC thrombus is limited by inflow artifact of unenhanced blood.

Magnetic resonance imaging is the modality of choice for the determination of the superior extent of IVC thrombus (ASLAM SOHAIB et al. 2002). The cephalad extent of tumor thrombus does not appear

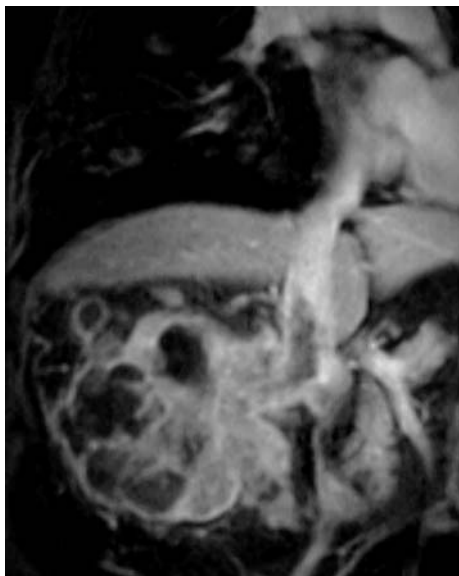


Fig. 4.20. Renal cell carcinoma in a 64-year-old man. Maximum intensity projection of coronal subtraction MRV (TR=4.7 ms, TE=1.6 ms) demonstrates avidly enhancing large right RCC with tumor thrombus in the right renal vein extending into the intrahepatic vena cava. No tumor thrombus above the diaphragm is seen.

to affect expected survival (MONTIE et al. 1991) but has a significant impact on surgical approach (OTO et al. 1998). Level-I thrombus extends into the IVC, no more than 2 cm above the renal vein confluence with the IVC, and can be removed through either a standard flank approach or an anterior approach. Level II extends more than 2 cm above the renal veins, but remains inferior to the hepatic veins, and requires an anterior approach through bilateral subcostal transperitoneal or thoracoabdominal incisions (Fig. 4.20). Level-III thrombus involves the intrahepatic IVC but remains below the diaphragm (Fig. 4.21). The surgical approach for level-III thrombus is transperitoneal and thoracoabdominal similar to level-II thrombus, but may additionally require cardiac bypass and hypothermic circulatory arrest. Level-IV thrombus involves the supra-diaphragmatic IVC or the right atrium. Excision of level-IV thrombus requires a median sternotomy, cardiac bypass, and hypothermic circulatory arrest, in addition to a transabdominal incision.

Renal vein anatomy is also assessed in candidates for radical nephrectomy. Normal variants such as the circum-aortic left renal vein (0.2–0.3%) and retro-aortic left renal vein (0.5–3%; Fig. 4.22) are readily demonstrable on MRV and should be reported as part of an overall MR imaging assessment of renal malignancy.

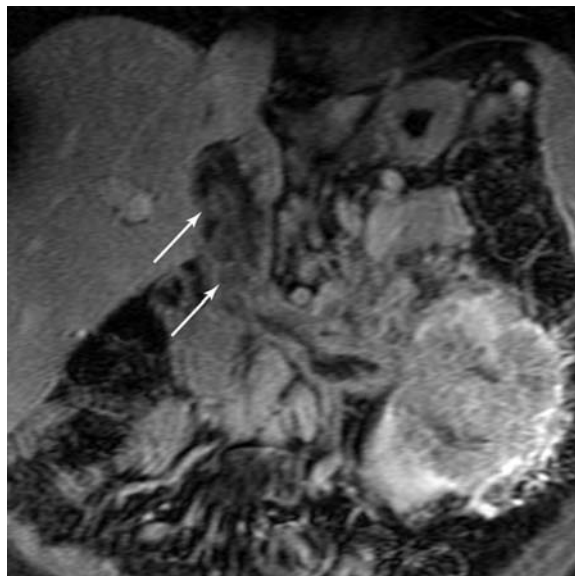


Fig. 4.21. Left renal cell carcinoma in a 44-year-old man. Coronal contrast-enhanced fat-suppressed T1-weighted GRE MR image (TR=6.5 ms, TE=2.2 ms) demonstrates a large left renal cell carcinoma. There is thrombus in the left renal vein and inferior vena cava. Nodular regions of enhancement (*arrows*) indicate that this is malignant thrombus. The superior extent of the caval thrombosis into the intrahepatic cava, but not above the hepatic veins, is clearly delineated.

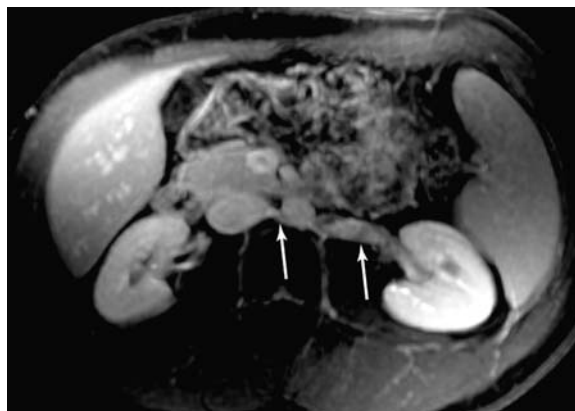


Fig. 4.22. Retro-aortic left renal vein in a 27-year-old man. Axial nephrographic phase contrast-enhanced fat-suppressed T1-weighted gradient echo MR image (TR=210 ms, TE=1.4 ms) demonstrates a retro-aortic left renal vein (*arrows*), a normal variant.

4.4.9 Flow-Related Vascular MR Imaging

Prior to development of contrast-enhanced breath-held MRA, time-of-flight imaging was a frequently used technique for evaluation of abdominal vasculature. Presently, however, time-of-flight renal vas-

cular imaging is unnecessary if one is performing a contrast-enhanced study, as it has significant disadvantages relative to contrast-enhanced MRA; these include long imaging times, signal loss due to in-plane flow, severe motion artifacts, and an inability to demonstrate the distal portion of renal arteries (NELSON et al. (1999).

Phase-contrast MR imaging has been used to quantify flow in evaluation of renal artery stenosis (BINKERT et al. 2001). It is not used in renal vascular imaging in the oncologic setting, due to long imaging times and numerous artifacts.

4.4.10

MR Urography

Magnetic resonance urography is probably unnecessary as part of routine evaluation of a renal mass, although it can be very useful as part of the evaluation of suspected transitional cell carcinoma, for renal donor evaluation (HUSSAIN et al. 2003), for imaging of renal transplants, and for imaging in patients who cannot receive iodine-based contrast agents (Fig. 4.23; CHU et al. 2004; EL-DIASTY et al. 2003). For this examination, 10 mg of furosemide (American Regent Laboratories, Shirley, N.Y.) is injected with the gadolinium chelate (NOLTE-ERNSTING et al. 1998). Mild diuresis with furosemide both mildly dilates the renal collecting system to facilitate imaging, and simultaneously prevents excreted gadolinium chelate from achieving high concentration, which could lead to T2* effect (Fig. 4.24; EL-DIASTY et al. 2003). Dynamic enhanced 3D images of the kidneys are acquired in arterial, venous, and nephrographic phases, and then the field of view is increased in the z plane to include the kidneys, ureters, and urinary bladder. Coronal 3D, breath-held, thin slab (2 mm interpolated to 1 mm) fat-suppressed T1-weighted GRE images are then acquired (3D EFGRE, GE Medical Systems; VIBE, Siemens Medical Solutions; Table 4.4). In situations where breath-hold imaging is not possible, respiratory-gated images can be acquired (ROHRSCHEIDER et al. 2002).

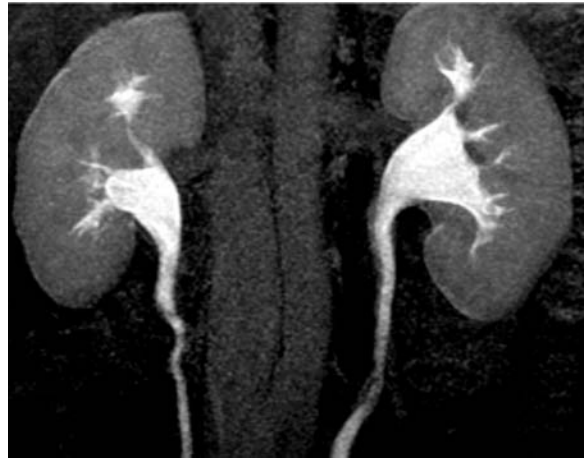


Fig. 4.23. Hematuria in a 39-year-old man. Coronal MIP reformatted MR image of 3D T1-weighted GRE excretory MR urogram (TR=5.5 ms, TE=1.1 ms) reveals normal collecting systems bilaterally.

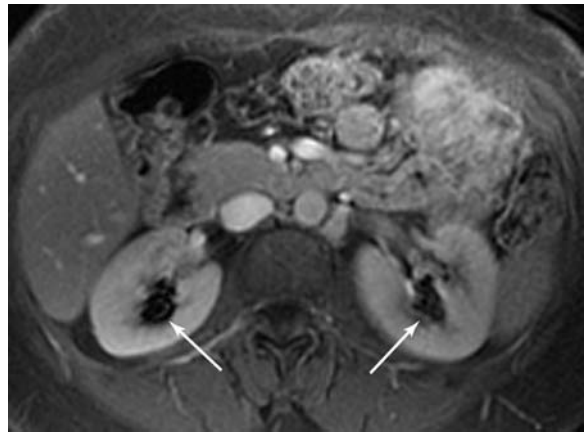


Fig. 4.24. Hematuria in a 42-year-old woman. Axial delayed contrast-enhanced fat-suppressed T1-weighted gradient-echo MR image (TR=150 ms, TE=1.4 ms) demonstrates markedly low hypointensity (arrows) within both renal collecting systems. This is the normal appearance of concentrated gadolinium chelate, and illustrates why furosemide is necessary to ensure excretion of a dilute and T1-hyperintense urine for T1-weighted excretory urography.

Table 4.4. Urothelial evaluation at 1.5 T MR scanner. NA not applicable

	Sequence	Plane	TR (ms)	TE (ms)	Flip angle(°)	FOV (cm)	Thickness (mm)	Matrix
Excretory MRU 3D	T1-GRE	Coronal	Minimum	Minimum	10	34	2 interpolated to 1	212/256
T2 Hydrography multislice	Half-Fourier T2	Coronal	NA	200	NA	36	5	256/256
T2 Hydrography thick slab	Half-Fourier T2	Coronal	NA	200	NA	36	70	256/256

Transitional cell carcinoma (TCC) is the second most common primary renal malignancy, although it is far more common in the urinary bladder than in the upper urinary tract. Between 30 and 75% of patients with upper tract TCC will have synchronous bladder tumors. Approximately 2–4% of patients with bladder TCC have synchronous upper tract disease (Fig. 4.25; MESSING and CATALONA 2000). Diagnosis of TCC, therefore, requires evaluation of the entire urothelium. Although MRU is capable of identifying large collecting system abnormalities (HUANG et al. 1994), it remains inferior to conventional excretory urography in the detection of small calyceal abnormalities (JUNG et al. 2000; NOLTE-ERNSTING et al. 1998).

Transitional cell carcinomas of the renal pelvis or renal collecting system are visualized on MRU or on T2-weighted images as filling defects, with or without proximal hydronephrosis (Fig. 4.26; KANEMATSU et al. 1996). In contrast to calculi, TCC will enhance following the administration of gadolinium chelate (WAGNER 1997), although tumors tend to enhance less than renal parenchyma. TCC is hypointense to urine on T2-weighted images. The MRU is known to be far inferior to unenhanced CT in detection of renal calculi, and the MRU identification of a non-enhancing filling defect in the renal collecting system is non-specific. Such a finding can represent stone, blood clot, gas bubble, or sloughed papilla (KAWASHIMA et al. 2003).

A second option for collecting system evaluation in hydronephrotic or non-functioning kidneys is heavily T2-weighted MR hydrography (SSFSE, GE Medical Systems; HASTE, Siemens Medical Solutions; Figs. 4.27, 4.28, 4.29; (Table 4.4; SHOKEIR et al. 2004). These are heavily T2-weighted sequences identical to those used for MR cholangiopancreatography (MRCP) and, like MRCP, can be performed



Fig. 4.26. Hematuria in a 66-year-old woman. Coronal T1-weighted gadolinium MRU (TR=6 ms, TE=0.8 ms) demonstrates a small, non-obstructing filling defect in the proximal left ureter (*arrow*). This was a transitional cell carcinoma.

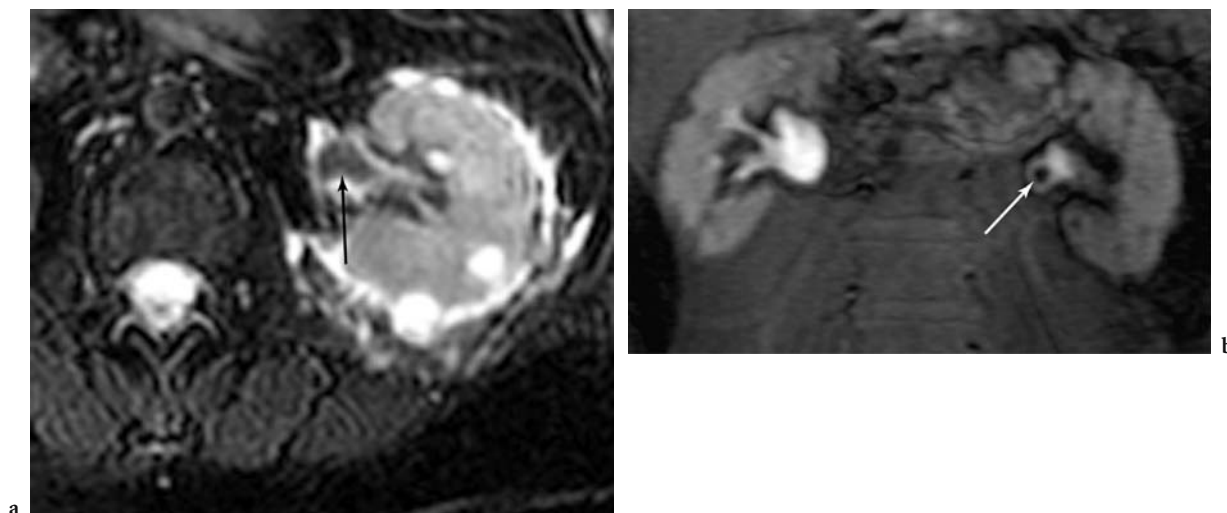


Fig. 4.25a,b. Transitional cell carcinoma of the left renal pelvis in an 82-year-old man. **a** Axial fat-suppressed respiratory-triggered fast-spin-echo T2-weighted MR image (TR=5700 ms, TE(eff)=106 ms) demonstrates a hypointense soft tissue mass (*arrow*) in the left renal pelvis. **b** Coronal T1-weighted gadolinium MRU (TR=5.5 ms, TE=1.2 ms) confirms the presence of a polypoid filling defect (*arrow*) in the left renal collecting system. The presence of enhancement within the lesion can be used to differentiate solid tumor masses from other potential causes of filling defects, including clot, stone, or air.



Fig. 4.27a,b. Obstructing transitional cell carcinoma at the left ureterovesical junction in a 67-year-old man. **a** Coronal half-Fourier T2-weighted MR image (TR=not significant, TE=92 ms) demonstrates left hydronephrosis. There is a suggestion of a soft tissue mass (*arrow*) at the left ureterovesical junction (UVJ), which was confirmed on other images. No filling defect is seen in the visualized portion of the upper tract urothelium. **b** Coronal T1-weighted gadolinium MRU (TR=6.3 ms, TE=1.4 ms) demonstrates excretion from the functioning right kidney and a normal-caliber right ureter. The obstructed left kidney (*arrows*) is not functioning.

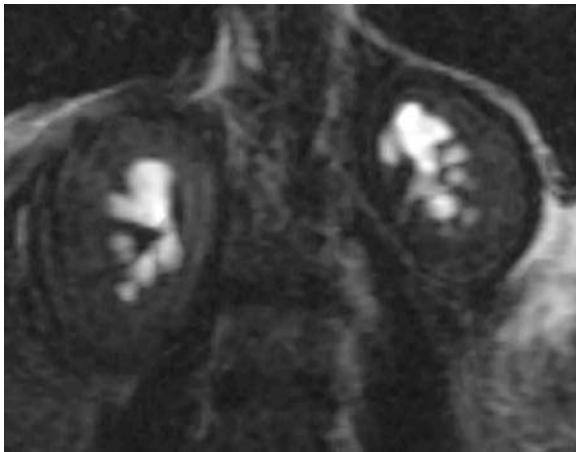


Fig. 4.28. Bilateral hydronephrosis in a 42-year-old woman. Coronal half-Fourier heavily T2-weighted MR hydrogram (TR=not meaningful, TE=431 ms) demonstrates fullness in both renal collecting systems. No calyceal or pelvic filling defect is present. In this case, hydronephrosis was due to compression from the patient's abnormal retroperitoneal soft tissue masses (not depicted), which were malignant histiocytes.

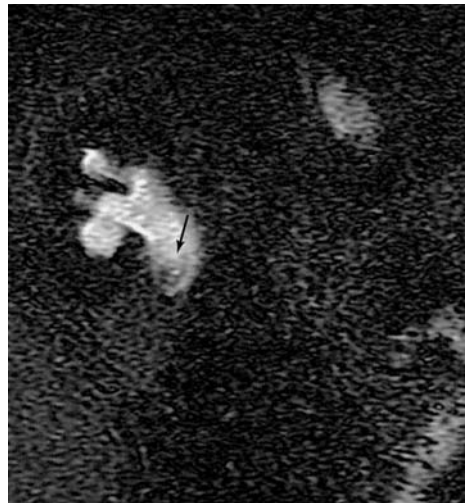


Fig. 4.29. Hematuria in a 56-year-old woman. Coronal half-Fourier heavily T2-weighted MR hydrogram (TR=not meaningful, TE=598 ms) demonstrates filling defect (*arrow*) in right renal pelvis resulting in hydronephrosis. This was obstructing transitional cell carcinoma.

as either multiple thin-section slices or as a single thick slab. Slices afford greater spatial information but, as single-shot half-Fourier images, have lower SNR (Fig. 4.29). These selected slices can then be viewed as an MIP projection to create a single image.

Thick-slab MRU creates a high SNR image, but high T2 signal intensity fluid in the bowel, the thecal sac, or in a dilated renal collecting system may obscure an urothelial tumor. These sequences can be useful in depicting an obstructed collecting system in a

non-functioning kidney, but if renal function exists, 3D T1-weighted images of the excreted gadolinium are preferred for detection and characterization of small stones and urothelial tumors with MR imaging (NOLTE-ERNSTING et al. 2001).

4.5 Conclusion

Magnetic resonance imaging is a powerful and versatile tool for single-modality evaluation of potential renal malignancies. A well-planned and executed high-field MR imaging examination can simultaneously detect and characterize a renal neoplasm. Multiphasic post-contrast imaging can generate MRA/MRV/MRU data sets with which, after post-processing, the radiologist can characterize the renal vasculature and stage the tumor. Magnetic resonance imaging also has an important role to play in helping clinicians to select the proper therapy for a renal tumor and in evaluating the patient following therapy. Ongoing advances in MR imaging, including the development of new pulse sequences, the increased availability of whole-body 3-T scanners, and the growing practicality of parallel imaging techniques will likely expand the role of MR imaging in imaging patients with known or suspected renal malignancies.

References

- Anzal Y, Piccoli CW, Outwater EK (2003) Evaluation of neck and body metastases to nodes with Furumoxtran 10-enhanced MR Imaging: phase III safety and efficacy study. *Radiology* 228:777–788
- Aslam Sohaib SA, Teh J, Nargund VH et al. (2002) Assessment of tumor invasion of the vena caval wall in renal cell carcinoma cases by magnetic resonance imaging. *J Urol* 167:1271–1275
- Balci NC, Semelka RC, Patt RH et al. (1999) Complex renal cysts: findings on MR imaging. *Am J Roentgenol* 172:1495–1500
- Bechtold RE, Zagoria RJ (1997) Imaging approach to staging of renal cell carcinoma. *Urol Clin North Am* 24:507–522
- Binkert CA, Debatin JF, Schneider E et al. (2001) Can MR measurement of renal artery flow and renal volume predict the outcome of percutaneous transluminal renal angioplasty? *Cardiovasc Intervent Radiol* 24:233–239
- Blute ML, Amling CL, Bryant SC et al. (2000) Management and extended outcome of patients with synchronous bilateral solid renal neoplasms in the absence of von Hippel-Lindau disease. *Mayo Clin Proc* 75:1020–1026
- Bono AV, Lovisolo JA (1997) Renal cell carcinoma-diagnosis and treatment: state of the art. *Eur Urol* 31 (Suppl 1):47–55
- Bosniak MA (1991) The small (≤ 3.0 cm) renal parenchymal tumor: detection, diagnosis, and controversies. *Radiology* 179:307–317
- Buzzas GR, Shield CF III, Pay NT et al. (1997) Use of gadolinium-enhanced, ultrafast, three-dimensional, spoiled gradient-echo magnetic resonance angiography in the preoperative evaluation of living renal allograft donors. *Transplantation* 64:1734–1737
- Bydder M, Larkman DJ, Hajnal JV (2002) Generalized SMASH imaging. *Magn Reson Med* 47:160–170
- Carroll TJ, Grist TM (2002) Technical developments in MR angiography. *Radiol Clin North Am* 40:921–951
- Casper KA, Donnelly LF, Chen B et al. (2002) Tuberosus sclerosis complex: renal imaging findings. *Radiology* 225:451–456
- Choyke PL (1997) Detection and staging of renal cancer. *Magn Reson Imaging Clin North Am* 5:29–47
- Choyke PL, Walther MM, Wagner JR et al. (1997) Renal cancer: preoperative evaluation with dual-phase three-dimensional MR angiography. *Radiology* 205:767–771
- Choyke PL, Dwyer AJ, Knopp MV (2003) Functional tumor imaging with dynamic contrast-enhanced magnetic resonance imaging. *J Magn Reson Imaging* 17:509–520
- Chu WC, Lam WW, Chan KW et al. (2004) Dynamic gadolinium-enhanced magnetic resonance urography for assessing drainage in dilated pelvicalyceal systems with moderate renal function: preliminary results and comparison with diuresis renography. *BJU Int* 93:830–834
- Clark PE, Schover LR, Uzzo RG et al. (2001) Quality of life and psychological adaptation after surgical treatment for localized renal cell carcinoma: impact of the amount of remaining renal tissue. *Urology* 57:252–256
- Corica FA, Iczkowski KA, Cheng L et al. (1999) Cystic renal cell carcinoma is cured by resection: a study of 24 cases with long-term followup. *J Urol* 161:408–411
- Corman JM, Penson DF, Hur K et al. (2000) Comparison of complications after radical and partial nephrectomy: results from the National Veterans Administration Surgical Quality Improvement Program. *BJU Int* 86:782–789
- Curry NS (2002) Imaging the small renal mass. *Abdom Imaging* 27:629–636
- D'Armiento M, Damiano R, Feleppa B (1997) Elective conservative surgery for renal carcinoma versus radical nephrectomy: a prospective study. *Br J Urol* 79:15–19
- Debatin JF, Sostman HD, Knelson M et al. (1993) Renal magnetic resonance angiography in the preoperative detection of supernumerary renal arteries in potential kidney donors. *Invest Radiol* 28:882–889
- DeKernion JB, Mukame E (1987) Selection of initial therapy for renal cell carcinoma. *Cancer* 60:539–546
- Dong Q, Schoenberg SO, Carlos RC et al. (1999) Diagnosis of renal vascular disease with MR angiography. *Radiographics* 19:1535–1554
- Edmunds TB Jr, Schulsinger DA, Durand DB et al. (2000) Acute histologic changes in human renal tumors after cryoablation. *J Endourol* 14:139–143
- Eilenberg SS, Lee JKT, Brown JJ et al. (1990) Renal masses: evaluation with gradient-echo Gd-DTPA-enhanced dynamic MR imaging. *Radiology* 176:333–338
- El-Diasty T, Mansour O, Farouk A (2003) Diuretic contrast-enhanced magnetic resonance urography versus intrave-

- nous urography for depiction of nondilated urinary tracts. *Abdom Imaging* 28:135–145
- El-Galley R (2003) Surgical management of renal tumors. *Radiol Clin North Am* 41:1053–1065
- Ergen FB, Hussain HK, Caoili EM et al. (2004) MRI for preoperative staging of renal cell carcinoma using the 1997 TNM classification: comparison with surgical and pathologic staging. *Am J Roentgenol* 182:217–225
- Fain SB, King BF, Breen JF et al. (2001) High spatial resolution contrast enhanced MR angiography of the renal arteries: a prospective comparisons with digital subtraction angiography. *Radiology* 218:481–490
- Farrell MA, Charboneau WJ, DiMarco DS et al. (2003) Imaging-guided radiofrequency ablation of solid renal tumors. *Am J Roentgenol* 180:1509–1513
- Fein AB, Lee JDT, Balfe DM et al. (1987) Diagnosis and staging of renal cell carcinoma. A comparison of MR imaging and CT. *Am J Roentgenol* 148:749–753
- Fergany AF, Hafez KS, Novick AC (2000) Long-term results of nephron sparing surgery for localized renal cell carcinoma: 10-year follow-up. *J Urol* 163:442–445
- Firmin D, Keegan J (2002) The use of navigator echoes in cardiovascular magnetic resonance and factors affecting their implementation. In: Manning WJ, Pennell DJ (eds) *Cardiovascular magnetic resonance*. Churchill Livingstone, Philadelphia, pp 186–195
- Gandy SJ, Sudarshan TA, Sheppard DG et al. (2003) Dynamic MRI contrast enhancement of renal cortex: a functional assessment of renovascular disease in patients with renal artery stenosis. *J Magn Reson Imaging* 18:461–466
- Ghavamian R, Zincke H (2001) Open surgical partial nephrectomy. *Semin Urol Oncol* 19:103–113
- Giessing M, Kroencke TJ, Taupitz M et al. (2003) Gadolinium-enhanced three-dimensional magnetic resonance angiography versus conventional digital subtraction angiography: Which modality is superior in evaluating living kidney donors? *Transplantation* 76:1000–1002
- Gofrit ON, Shapiro A, Kovalski N et al. (2001) Renal cell carcinoma: evaluation of the 1997 TNM system and recommendations for follow-up after surgery. *Eur Urol* 39:669–674
- Guillonneau B, Bermudez H, Gholami S et al. (2001) Laparoscopic partial nephrectomy for renal tumor: single center experience comparison clamping and no clamping techniques of the renal vasculature. *J Urol* 169:483–486
- Hafex KS, Fergany AF, Novick AC et al. (1999) Nephron sparing surgery for localized renal cell carcinoma: impact of tumor size on patient survival, tumor recurrence and TNM staging. *J Urol* 162:1930–1933
- Halpern EJ, Mitchell DG, Wechsler RJ et al. (2000) Preoperative evaluation of living renal donors: comparison of CT angiography and MR angiography. *Radiology* 216:434–439
- Hartman DS, Weatherby E III, Laskin WB et al. (1986) Cystic renal cell carcinoma. *Urology* 28:145–158
- Hayes C, Padhani AR, Leach MO (2002) Assessing changes in tumor vascular function using dynamic contrast-enhanced magnetic resonance imaging. *NMR Biomed* 15:154–163
- Heidemann RM, Ozsarlak O, Parizel PM et al. (2003) A brief review of parallel magnetic resonance imaging. *Eur Radiol* 13:2323–2337
- Heiss SG, Shifrin RY, Sommer FG (2000) Contrast-enhanced three-dimensional fast spoiled gradient-echo renal MR imaging: evaluation of vascular and nonvascular disease. *Radiographics* 20:1341–1352
- Helenon O, Merran S, Paraf F et al. (1997) Unusual fat-containing tumors of the kidney: a diagnostic dilemma. *Radiographics* 17:129–144
- Hinshaw JL, Lee Jr FT (2004) Image-guided ablation of renal cell carcinoma. *Magn Reson Imaging Clin North Am* 12:429–448
- Ho VB, Allen SF, Hood MN et al. (2002) Renal masses: quantitative assessment of enhancement with dynamic MR imaging. *Radiology* 224:695–700
- Hollenbeck BK, Wolf JS Jr (2001) Laparoscopic partial nephrectomy. *Semin Urol Oncol* 19:123–132
- Hosokawa Y, Kinouchi T, Sawai Y et al. (2002) Renal angiomyolipoma with minimal fat. *Int J Clin Oncol* 7:120–123
- Hricak H, Thoeni RF, Carroll R (1988) Detection and staging of renal neoplasms: a reassessment of MR imaging. *Radiology* 166: 643–649
- Huang AJ, Lee VS, Rusinek H (2003) MR imaging of renal function. *Radiol Clin North Am* 41:1001–1017
- Huang AJ, Lee VS, Rusinek H (2004) Functional renal MR imaging. *Magn Reson Imaging Clin N Am* 12:469–486
- Huang CL, Liu GC, Sheu RS et al. (1994) Magnetic resonance imaging and computed tomography of transitional cell carcinoma of renal pelvis and ureter. *Gaoxiong Yi Xue Ke Xue Za Zhi* 10:194–202
- Hussain SM, Kock MC, Ijzermans JN et al. (2003) MR imaging: a "one-stop shop" modality for preoperative evaluation of potential living kidney donors. *Radiographics* 23:505–520
- Israel GM, Bosniak MA (2003a) Follow-up CT of moderately complex cystic lesions of the kidney (Bosniak category IIF). *Am J Roentgenol* 181:627–633
- Israel GM, Bosniak MA (2003b) Renal imaging for diagnosis and staging of renal cell carcinoma. *Urol Clin North Am* 30:499–514
- Israel GM, Bosniak MA (2004) MR imaging of cystic renal masses. *Magn Reson Imaging Clin N Am* 12:403–412
- Itano NB, Blute ML, Spotts B et al. (2000) Outcome of isolated renal cell carcinoma fossa recurrence after nephrectomy. *J Urol* 164:322–325
- Janetschek G, Daffner P, Peschel R et al. (1998) Laparoscopic nephron sparing surgery for small renal cell carcinoma. *J Urol* 159:1152–1155
- Jinzaki M, Tanimoto A, Narimatsu Y et al. (1997) Angiomyolipoma: imaging findings in lesions with minimal fat. *Radiology* 205:497–502
- John G, Semelka RC, Burdeny DA et al. (1997) Renal cell cancer: incidence of hemorrhage on MR images in patients with chronic renal insufficiency. *J Magn Reson Imaging* 7:157–160
- Jung P, Brauers A, Nolte-Ernsting CA et al. (2000) Magnetic resonance urography enhanced by gadolinium and diuretics: a comparison with conventional urography in diagnosing the cause of ureteric obstruction. *BJU Int* 86:960–965
- Kallman DA, King BF, Hattery RR et al. (1992) Renal vein and inferior vena cava thrombus in renal cell carcinoma: CT, US, MRI and venacavagraphy. *J Comput Assist Tomogr* 16:240–247
- Kanematsu M, Hoshi H, Imaeda T et al. (1996) Renal pelvic and ureteral carcinoma with huge hydronephrosis: US, CT, and MR findings. *Radiat Med* 14:321–323
- Kawashima A, Glockner JF, King Jr BF (2003) CT urography and MR urography. *Radiol Clin N Am* 41:945–961
- Kearney GP, Waters RB, Klein LA et al. (1981) Results of IVC resection for renal cell carcinoma. *J Urol* 125:769–773

- Kocak M, Sudakoff GS, Erickson S et al. (2001) Using MR angiography for surgical planning in pelvic kidney renal cell carcinoma. *Am J Roentgenol* 177:659–660
- Laissy JP, Menegazzo D, Debray MP et al. (2000) Renal carcinoma: diagnosis of venous invasion with Gd-enhanced MR venography. *Eur Radiol* 10:1138–1143
- Lewin JS, Connell CF, Duerk JL et al. (1998) Interactive MRI-guided radiofrequency interstitial thermal ablation of abdominal tumors: clinical trial for evaluation of safety and feasibility. *J Magn Reson Imaging* 8:40–47
- Licht MR, Novick AC, Goormastic M (1994) Nephron-sparing surgery in incidental versus suspected renal cell carcinoma. *J Urol* 152:39–42
- Lin FH, Kwong KK, Belliveau JW et al. (2004) Parallel imaging reconstruction using automatic regularization. *Magn Reson Med* 51:559–567
- Lockhart ME, Smith JK (2003) Technical considerations in renal CT. *Radiol Clin North Am* 41:863–875
- Low RN, Martinez AG, Steinberg SM et al. (1998) Potential renal transplant donors: evaluation with gadolinium-enhanced MR angiography and MR enhanced MR angiography. *Am J Roentgenol* 177:349–355
- Maki DD, Birnbaum BA, Chakraborty DP et al. (1999) Renal cyst pseudo-enhancement: beam hardening effects on CT attenuation values. *Radiology* 213:468–472
- McKenzie CA, Lim D, Ransil BJ et al. (2004) Shortening MR image acquisition time for volumetric interpolated breath-hold examination with a recently developed parallel imaging reconstruction technique: clinical feasibility. *Radiology* 230:589–594
- Messing EM, Catalona W (2000) Urothelial tumors of the urinary tract. In: Walsh PC, Retik AB, Vaughan ED Jr, Wein AJ (eds) *Campbell's urology*, 7th edn. Saunders, Philadelphia, pp 2385–2387
- Meyers SP, Talagala SL, Totterman S et al. (1995) Evaluation of the renal arteries in kidney donors: value of three-dimensional phase-contrast MR angiography with maximum-intensity-projection or surface rendering. *Am J Roentgenol* 164:117–121
- Montie JE, Pontes JE, Novick AC et al. (1991) Resection of IVC tumor thrombi from renal cell carcinoma. *Am Surg* 57:56–61
- Murphy DP, Gill IS (2001) Energy-based renal tumor ablation: a review. *Semin Urol Oncol* 19:133–140
- Naito S, Nakashima M, Kimoto Y et al. (1998) Application of microwave tissue coagulator in partial nephrectomy for renal cell carcinoma. *J Urol* 159:960–962
- Nascimento AB, Mitchell DG, Zhang XM et al. (2001) Rapid MR imaging detection of renal cysts: age-based standards. *Radiology* 221:628–632
- Nelson HA, Gilfeather M, Holman JM et al. (1999) Gadolinium-enhanced breathhold three-dimensional time-of-flight renal MR angiography in the evaluation of potential renal donors. *J Vasc Interv Radiol* 10:175–181
- Nguyen BD, Westra WH, Zerhouni EA (1996) Renal cell carcinoma and tumor thrombus neovascularity: MR demonstration with pathologic correlation. *Abdom Imaging* 21:269–271
- Nolte-Ernsting CC, Bucker A, Adam GB et al. (1998) Gadolinium-enhanced excretory MR urography after low-dose diuretic injection: comparison with conventional excretory urography. *Radiology* 209:147–157
- Nolte-Ernsting CC, Adam GB, Gunther RW (2001) MR urography: examination techniques and clinical applications. *Eur Radiol* 11:355–372
- Norris DG (2003) High field human imaging. *J Magn Reson Imaging* 18:519–529
- Oto A, Herts BR, Remer EM et al. (1998) Inferior vena cava tumor thrombus in renal cell carcinoma: staging by MR imaging and impact on surgical treatment. *Am J Roentgenol* 171:1619–1624
- Outwater EK, Bhatia M, Siegelman ES et al. (1997) Lipid in renal clear cell carcinoma: detection on opposed-phase gradient-echo MR images. *Radiology* 205:103–107
- Outwater EK, Blasbalg R, Siegelman ES et al. (1998) Detection of lipid in abdominal tissues with opposed-phase gradient-echo images at 1.5 T: techniques and diagnostic importance. *Radiographics* 18:1465–1480
- Patel SK, Stack CM, Turner DA (1987) Magnetic resonance imaging in staging of renal cell carcinoma. *Radiographics* 7:703–728
- Pretorius ES, Siegelman ES, Ramchandani P et al. (1999) Renal neoplasms amenable to partial nephrectomy: MR imaging. *Radiology* 212:28–34
- Ramdave S, Thomas GW, Berlangieri SU et al. (2001) Clinical role of F-18 fluorodeoxyglucose positron emission tomography for detection and management of renal cell carcinoma. *J Urol* 166:825–830
- Rankin SC, Jan W, Koffman CG (2001) Noninvasive imaging of living related kidney donors: evaluation with CT angiography and gadolinium-enhanced MR angiography. *Am J Roentgenol* 177:349–355
- Rassweiler JJ, Abbou C, Janetschek G et al. (2000) Laparoscopic partial nephrectomy. The European experience. *Urol Clin North Am* 27:721–736
- Remer EM, Weinberg EJ, Oto A (2000) MR imaging of the kidneys after laparoscopic cryoablation. *Am J Roentgenol* 174:635–640
- Reznek RH (1996) Imaging in the staging of renal cell carcinoma. *Eur Radiol* 6:120–128
- Robson CJ, Churchill BM, Anderson W (1969) The results of radical nephrectomy for renal cell carcinoma. *J Urol* 101:297–301
- Rofsky NM, Bosniak MA (1997) MR imaging in the evaluation of small (≤ 3.0 cm) renal masses. *Magn Reson Imaging Clin N Am* 5:67–81
- Rofsky NM, Lee VS, Laub G et al. (1999) Abdominal MR imaging with a volumetric interpolated breath-hold examination. *Radiology* 212:876–884
- Rohrschneider WK, Haufwe S, Wiesel M et al. (2002) Functional and morphologic evaluation of congenital urinary tract dilation by using combined static-dynamic MR urography: findings in kidneys with a single collecting system. *Radiology* 224:683–694
- Sewell PE, Howard JC, Shingleton WB et al. (2003) Interventional magnetic resonance image-guided percutaneous cryoablation of renal tumors. *South Med J* 96:708–710
- Shinmoto H, Yuasa Y, Tanimoto A et al. (1998) Small renal cell carcinoma: MRI with pathologic correlation. *J Magn Reson Imaging* 8:690–694
- Shokeir AA, El-Diasty T, Eassa W et al. (2004) Diagnosis of noncalcareous hydronephrosis: role of magnetic resonance urography and noncontrast computed tomography. *Urology* 63:225–229
- Silverman SG, Lee BY, Seltzer SE et al. (1994) Small (< 3 cm) renal masses: correlation of spiral CT features and pathologic findings. *Am J Roentgenol* 163:597–605

- Sodickson DK (2002) Clinical cardiovascular magnetic resonance imaging techniques. In: Manning WJ, Pennell DJ (eds) Cardiovascular magnetic resonance. Churchill Livingstone, Philadelphia. pp 18–30
- Steinbach F, Stöckle M, Hohenfellner R (1995) Current controversies in nephron sparing surgery for renal cell carcinoma. *World J Urol* 13:163–165
- Steiner MS, Quinlan D, Goldman SM et al. (1990) Leiomyomas of the kidney: presentation of 4 new cases and the role of computerized tomography. *J Urol* 143:994–998
- Teh HS, Ang ES, Wong WC et al. (2003) MR renography using a dynamic gradient-echo sequence and low-dose gadopentetate dimeglumine as an alternative to radionuclide renography. *Am J Roentgenol* 181:441–450
- Tsui KH, Shvarts O, Smith RB et al. (2000) Renal cell carcinoma: prognostic significance of incidentally detected tumors. *J Urol* 163:426–430
- Van den Brink JS, Watanabe Y, Kuhl CK et al. (2003) Implications of SENSE MR in routine clinical practice. *Eur J Radiol* 46:3–27
- Wagner BJ (1997) The kidney: radiologic–pathologic correlation. *Magn Reson Imaging Clin N Am* 5:13–28
- Wagner BJ, Wong-You-Cheong JJ, Davis CJ Jr (1997) Adult renal hamartomas. *Radiographics* 17:155–169
- Wilman AH, Riederer SJ (1997) Performance of an elliptical centric view order for signal enhancement and motion artifact suppression in breath-hold three-dimensional gradient echo imaging. *Magn Reson Med* 38:793–802
- Yamashita Y, Miyazaki T, Hatanaka Y et al. (1995) Dynamic MRI of small renal cell carcinoma. *J Comput Assist Tomogr* 19:759–765
- Yoshimura K, Okubo K, Ichioka K et al. (2001) Laparoscopic partial nephrectomy with a microwave tissue coagulator for small renal tumor. *J Urol* 165:1893–1896
- Zagoria RJ (2003) Percutaneous image-guided radiofrequency ablation of renal malignancies. *Radiol Clin North Am* 41:1067–1075
- Zagoria RJ, Bechtold RE (1997) The role of imaging in staging renal adenocarcinoma. *Semin Ultrasound CT MR* 18:91–99
- Zhang H, Prince MR (2004) Renal MR angiography. *Magn Reson Imaging Clin N Am* 12:487–504
- Zhang J, Pedrosa I, Rofsky NM (2003) MR techniques for renal imaging. *Radiol Clin North Am* 41:877–907